1957BAN....13..201W

THE DISTRIBUTION OF ATOMIC HYDROGEN IN THE OUTER PARTS OF THE GALACTIC SYSTEM

BY G. WESTERHOUT

A three-dimensional picture of the distribution of neutral hydrogen in the Galactic System beyond 8.2 kpc from the centre is obtained from a set of 620 profiles of the 21-cm line, measured at Kootwijk from $l = 340°$ to 220° and $b = +10°$ to $-10°$. The effects that tend to broaden the line profile are discussed in Part I, while in Part II the reduction methods applied to the profiles are given. The profiles have been corrected for the smoothing effect of the 37 kc/s bandwidth of the receiver by means of EDDINGTON's approximation to the solution of the smoothing integral. Corrections have also been applied for the antenna pattern with $2°.78 \times 1°.85$ beamwidth. In converting intensity into optical depth it was assumed that the neutral hydrogen has a constant temperature of 125°K throughout the parts of the Galactic System studied here. The effect of this assumption on the results is discussed. It was not found possible in the present investigation to assume different values for the dispersion of the random cloud velocities in different regions. The distribution of these random velocities appears to resemble a gaussian distribution with a dispersion of 6 km/sec. The profiles are corrected for this dispersion with the help of EDDINGTON's approximation. A model of the mass distribution in the Galactic System, computed by M. SCHMIDT, was used for converting radial velocities into distances (Table 1). The hydrogen densities are plotted as density contours in planes through the Sun, perpendicular to the galactic plane (Figure 9, pp. 223 to 246). The maximum densities in the z-direction are plotted in Plate B. Plate A is a sketch of all details concerning the interconnection and shape of the spiral arms, determined from a study of the cross sections. The Orion arm and the Perseus arm are the two major arms, while two intermediate arms are visible. Outside the Perseus arm, faint outer arms extend as far as 12.5 to 15 kpc from the centre. In Figure 8 the corrected optical depths in the region $l = 135°$ to 160°, where conversion into distance is not possible, are plotted as a function of radial velocity. From the data obtained in this and the following paper a mean galactic plane is determined. The points of maximum density with $R < 8$ kpc appear to have a much more regular distribution in the z-direction than those with $R > 8$ kpc. When the former points are given the largest weight, the galactic pole as determined from these measurements is $l = 322°$, $b = 88°.56$. In the outer parts of the system, systematic deviations from the plane to more than 300 pc are found (Figure 7).

1. *Introduction.*

The article describes the reduction of 21-cm line profiles, obtained with the Kootwijk receiver between November 1953 and August 1955. The parts of the Galactic System which lie outside a circle with radius 8.2 kpc, i.e. farther from the centre than the sun, will be called the "outer parts". A three-dimensional picture of those parts can be obtained by studying the profiles in the region $l = 220°$ to $l = 57°.5$ fully and the profiles between $l = 55°$ and $l = 340°$ only at frequencies that originate in the "outer parts".

In total, approximately 620 line profiles [1]) have been studied, which may be divided into three groups.

a. From $l = 340°$ to $l = 42°.5$, at $2\frac{1}{2}$-degree intervals in galactic longitude. The latitude intervals are approximately 2 degrees from $b = -5°.5$ to $b = +4°.5$, along declination circles. The exact positions of these profiles are given in Table 1 of the first paper of this series (p. 159).

b. From $l = 45°$ to $l = 110°$, at $2\frac{1}{2}$-degree intervals in l and $2\frac{1}{2}$-degree intervals in b from $b = -10°$ to $b = +10°$, along lines perpendicular to the galactic equator. At some longitudes, the latitude range was extended to $\pm 12°.5$ or 15°.

c. From $l = 115°$ to $l = 220°$, at 5-degree intervals in l and $2\frac{1}{2}$-degree intervals in b from $b = -10°$ to $+10°$.

From each profile, the distribution of neutral hydrogen as a function of the distance to the sun may be derived. A combination of all profiles results in a three-dimensional picture of the hydrogen density, and may be given as contour diagrams representing cross-sections in planes perpendicular to the galactic plane.

For much of the theoretical background, as well as for many optical data concerning galactic rotation, the reader is referred to *B.A.N.* No. 452 [2]), where the hydrogen distribution in the galactic plane was derived from a study of line profiles at $b = 0°$. The present article is based on completely new data, both in the plane and at higher latitudes.

PART I

BROADENING EFFECTS AND THEIR REDUCTION

2. *General.*

The 21-cm spectral line, emitted by a group of clouds consisting of H-atoms, is subject to various changes in frequency and intensity before it is registered by the instrument. These effects may be summarized as follows.

a. Thermal motion of the atoms in a cloud.

b. Random motion of the clouds of a group with respect to their local centre of gravity.

c. Differential galactic rotation.

d. Deviations from circular motion around the galactic centre, hereafter called group motion.

e. Motions of the earth and the sun with respect to the local centre of gravity.

f. Selfabsorption.

g. The absorption of continuous background radiation, including that from point sources, influencing the registered intensity of the line because of instrumental effects.

[1]) C. A. MULLER and G. WESTERHOUT, *B.A.N.* **13**, 151 (No. 475, first paper), 1957.

[2]) H. C. VAN DE HULST, C. A. MULLER and J. H. OORT, *B.A.N.* **12**, 117 (No. 452), 1954.

© Astronomical Institutes of The Netherlands • Provided by the NASA Astrophysics Data System

1957BAN..13..201W

h. Extinction and earth radiation at positions close to the horizon.
i. Width of the antenna pattern.
j. Bandwidth.
k. Combined effect of time constant and sweeping speed in frequency.

The effects $a - d$ affect the frequency and thus influence the number of atoms from which radiation is received in a certain frequency interval. The effects $f - k$ mainly influence the intensity of the incoming radiation and the reading of the recording meter. The effect of the motions of earth and sun (*e*) introduces only a frequency shift of the whole line. The delaying effect of the time constant is visible as a frequency shift, due to the sweeping in frequency (*k*).

The effects *e*, *h* and *k* have already been eliminated from the line profiles catalogued in the first paper. We shall now discuss the other effects and methods to correct the line profiles.

3. *The bandwidth of the receiver.*

The pass band of the receiver is nearly gaussian in shape and may be represented by

$$\frac{8}{3a\pi}\left(1+\frac{x^2}{a^2}\right)^{-3}$$

where $a = 31.5$ kc/s. The noise bandwidth (equivalent width of the pass band) is 37 kc/s, while the width between half-power points is 33 kc/s. It broadens the line profile and obliterates any detail that is considerably smaller than the bandwidth. It is obvious that such detail cannot be present in the observed curves, and that also the resulting detail in the hydrogen densities is limited to a certain size. Translating the 37 kc/s bandwidth into linear distance at, say, $l = 60°$, and assuming that the smallest detail observable is $\frac{1}{2}$ bandwidth, it follows that this limit is of the order of 300 pc (see Table 3).

As will be shown later, this limit is considerably smaller than the limit set by the other broadening mechanism, i.e. the random cloud velocities. The smoothing effect of the bandwidth may be represented by the integral equation

$$h(\nu) = \frac{8}{3a\pi}\int_{-\infty}^{\infty} h'(\nu_0)\left\{1+\frac{(\nu-\nu_0)^2}{a^2}\right\}^{-3} d\nu_0 \qquad (1)$$

where $h'(\nu)$ is the profile coming into the receiver and $h(\nu)$ is the profile after smoothing.

To correct the curves for this effect, a solution for the integral equation has to be found. The well-known EDDINGTON approximation,

$$h'(\nu) = h(\nu) - c\frac{d^2h}{d\nu^2} \qquad (2)$$

is permissible if the smoothing function has a much smaller width than the integral itself. This condition is fulfilled, provided that we do not want to detect individual clouds, which have a very narrow velocity distribution. In general, the halfwidths of peaks in the line profiles are of the order of 100 kc/s. The solution may be further approximated by taking second differences instead of differentials,

$$h'(\nu) = h(\nu) - \varepsilon_B \Delta^2 h(\nu),$$

where $\varepsilon_B = c/\Delta\nu^2$ and the frequency interval over which the differences are taken is $\Delta\nu$. In some deep valleys between two tops, the halfwidth of the profile becomes of the same order as the bandwidth, and the EDDINGTON approximation is no longer permitted.

We now have to find the value of the constant ε_B in the approximation. OLLONGREN and VAN DE HULST [1]) have shown, that a convenient comparison of various solution methods may be made by plotting the Fourier transforms of the resolving functions. Adopting the terminology of their paper, the resolving function $B(\varphi)$, which is the Fourier transform of the inverse operator of the function describing the pass band, may be written as

$$B(\varphi) = \frac{3}{3 + 3a\varphi + a^2\varphi^2} \cdot e^{a\varphi}. \qquad (3)$$

The Fourier transform of the resolving function used in EDDINGTON's method with second differences is

$$B'(\varphi) = 1 + 2\varepsilon_B(1 - \cos\varphi\Delta\nu). \qquad (4)$$

Developing both functions into a power series we find in the second-order approximation $\varepsilon_B = \frac{1}{6}\, a^2/\Delta\nu^2$. The frequency interval used for determining second differences, throughout the present work, was $\Delta\nu = 20$ kc/s $= 4.2$ km/sec. With $a = 31.5$ kc/s we find $\varepsilon_B = 0.41$.

FIGURE 1

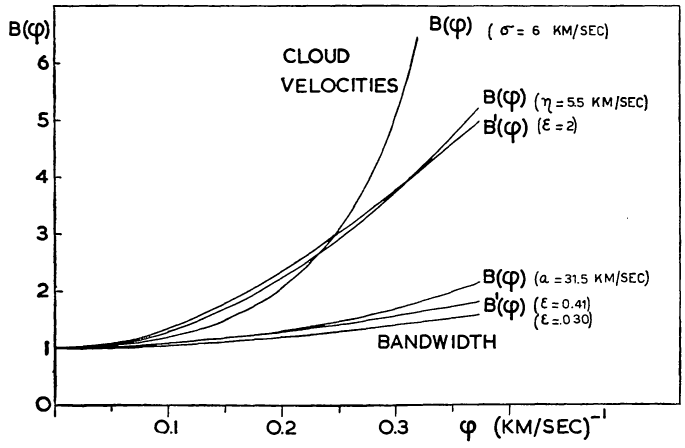

Fourier transforms of the reduction methods for bandwidth and cloud velocities. B(φ) are the exact, B'(φ) the approximate operators.

[1]) A. OLLONGREN and H. C. VAN DE HULST, *B.A.N.* **13**, 196 (No. 475, second paper), 1957.

© Astronomical Institutes of The Netherlands • Provided by the NASA Astrophysics Data System

1957BAN....13..201W

A comparison of $B(\varphi)$ and $B'(\varphi)$ for $\varepsilon_B = 0.41$ (Figure 1) shows that up to about $\varphi = 0.20 - 0.25$ the two operators are nearly identical. At $\varphi = 0.3$ the correct operator $B(\varphi)$ is appreciably larger than the approximate $B'(\varphi)$. Thus, for periods down to $\frac{2\pi}{0.23} = 27$ km/sec or 130 kc/s in the line profiles, corresponding to peak-to-valley distances or halfwidths down to 65 kc/s, the EDDINGTON approximation comes very close to the correct value. As halfwidths smaller than this value do not occur in the line profiles, EDDINGTON's approximation may be used.

Unfortunately, at the time the bandwidth corrections were started, we did not realize that the shape of the pass band, although nearly gaussian in the top, deviates fairly much from a gaussian curve in the wings. In the reductions, we assumed that it had the form

$$\frac{1}{\sigma\sqrt{2\pi}} e^{-\nu^2/2\sigma^2} .$$

The Fourier transform of the inverse operator then is $B(\varphi) = e^{+\varphi^2\sigma^2/2}$ and with $\sigma = 16$ kc/s, corresponding to a halfwidth of 37 kc/s, $\varepsilon_B = \sigma^2/2\Delta\nu^2 = 0.3$.

The value $\varepsilon_B = 0.3$ has been used throughout the reductions, giving the reduction formula $h'(\nu) = h(\nu) - 0.3\ \Delta^2 h(\nu)$. There is a difference of a factor 1.4 between the exact resolving function and the resolving function used, as shown in Figure 1. If we would have used the correct value $\varepsilon_B = 0.41$, some sharp details would have stood out more pronouncedly. In view of the smallness of the correction, however, the effect of this error is not too serious. Only in extreme cases (sharp tops) the corrections to $h(\nu)$ with the method used exceed 10% and most are far below this value.

It is of interest to note that a comparison between one of our line profiles with one made at Harvard (see also section 13a), shows that the Leiden curve, if corrected for the 37 kc/s bandwidth with $\varepsilon_B = 0.3$, is very similar to the Harvard curve obtained with a 15 kc/s bandwidth.

The importance of the bandwidth correction was realized only after the reduction of a considerable number of profiles was completed. Logically, the bandwidth correction should be applied to the measured profile before any other reductions. It was, however, found possible to apply the correction after all other corrections. Part of the profiles have been corrected in this order (section 13a).

4. *The antenna pattern.*

Throughout the reductions the antenna pattern was assumed to have a gaussian shape and an elliptical cross-section with widths between half-power points of 2°.7 and 1°.9. This assumption was based on rough measurements of transits of the sun. Later, a number of sweeps through the radio source Cassiopeia A were obtained with a continuum receiver working at a wave length of 22 cm; the shape of the pattern appeared to be very nearly gaussian indeed, with halfwidths of 2°.78 and 1°.85 (Figure 2). The

FIGURE 2

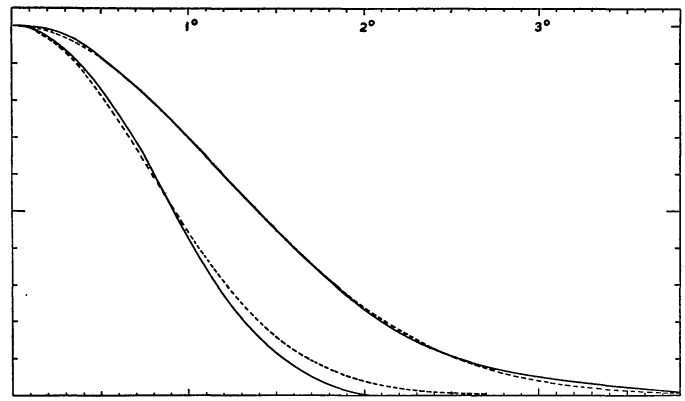

Main lobe of the antenna pattern in two perpendicular directions. ------ Gaussian curves.

influence of the width of the antenna pattern on the measured intensity is rather complex: the intensity distribution across the sky is different for each frequency in the line. Therefore, if corrections are made for the smoothing effect, these will have to be made at small frequency intervals. The intervals chosen here were 40 kc/s.

A second difficulty lies in the fact, that the antenna pattern is strongly elliptical. If corrections are to be found by comparing line profiles in adjacent regions, all line profiles should be obtained with the antenna pattern making a constant angle with the galactic equator. Because the antenna was azimuthally mounted, this implied measuring adjacent line profiles at approximately the same sidereal time. In cases where this was not done, a compromise had to be found, giving larger weight to the profiles with the highest intensities. Theoretically, a two-dimensional correction would have to be applied, but in practice this did not seem necessary as most features have a fairly large extension in the co-ordinate parallel to the galactic equator; most spiral arms run parallel to the galactic plane.

It was decided, therefore, to apply corrections only in the co-ordinate perpendicular to the galactic equator. The width of the intensity distribution in this direction is much smaller than that in the longitudinal direction, but even so it was generally much wider than the antenna pattern.

The reduction problem is the same as for the band-

© Astronomical Institutes of The Netherlands • Provided by the NASA Astrophysics Data System

1957AN....13..203W

width corrections: a solution has to be found for the smoothing integral. Again, the EDDINGTON approximation proved useful; it was applied nearly always when the width between half-intensity points of the latitude distribution was larger than 5° (i.e. twice the antenna pattern). The antenna pattern may be represented by

$$\frac{1}{1.065\,A}\cdot e^{\left(\frac{1.665}{A}b\right)^2}, \qquad (5)$$

where A is the effective halfwidth in the latitude direction. EDDINGTON's approximation in this case is

$$i(b) = h(b) - \varepsilon_A \Delta^2 h(b)\,, \qquad (6)$$

with $\varepsilon_A = \sigma^2/2\,\Delta b^2 = A^2/11.1\,\Delta b^2$.

When the halfwidth of the latitude distribution was smaller than 5°, application of this approximation introduced too large an error, and another method was used. A gaussian curve with halfwidth W was fitted into the distribution curve, so that this curve could be described by

$$h(b) = h_{\text{top}}\, e^{-\left\{\frac{1.665}{W}(b-b_{\text{top}})\right\}^2} + r(b)\,. \qquad (7)$$

The rest-curve $r(b)$ usually was a very flat curve. The smoothing integral may now be solved in two parts. The solution of the first part is gaussian again,

$$g'(b) = \frac{W}{G}\,h_{\text{top}}\, e^{-\left\{\frac{1.665}{G}(b-b_{\text{top}})\right\}^2} \qquad (8)$$

where G is the halfwidth of the resulting curve, $G = \sqrt{W^2 - A^2}$. The solution of the second part may be approximated safely by EDDINGTON's method, thus giving

$$r'(b) = r(b) - \varepsilon_A \Delta^2 r(b)\,. \qquad (9)$$

The corrected latitude distribution is the sum of the two partial solutions, (8) + (9), $i(b) = g'(b) + r'(b)$.

It should be realized that this elaborate method is necessary only if: *a.* the latitude distribution is very sharp, *b.* the longitude distribution is very flat, so that its influence can be neglected. In view of uncertainties in the relative intensities of adjacent line profiles, although smaller than 5%, and in view of the fact that the longitude distribution is not completely flat, it is doubtful whether this method was necessary in the majority of cases.

The values of the correction factors in the top of the latitude distribution usually varied between 1.04 and 1.15 with 1.30 in extreme cases. Tests by using both methods, taking also the longitude distribution into account, showed that the uncertainty in these factors was of the order of ± 0.05.

5. *Absorption and optical depth.*

It has been shown in *B.A.N.* No. 452 (section 16) that the optical depth of a column of neutral hydrogen atoms of 1 cm² cross section at a certain frequency corresponding to a radial velocity V, is

$$\tau(\nu) = \frac{N(V)}{1.835 \times 10^{13} T}, \qquad (10)$$

where $N(V)$ is the number of atoms per cm/sec velocity interval in the column and T their kinetic temperature. Frequency and radial velocity are connected by the Doppler law $d\nu = \frac{\nu}{c}\,dV$. If ν is expressed in kc/s (ν = 1420405.6 kc/s) and V in km/sec (c = 299791 km/sec), this gives $d\nu = 4.738\,dV$. In the present reductions, and in all former publications, c was taken 300000 km/sec, which gives $\nu/c = 4.735$. The difference with the correct value does not influence the reduction.

The intensity received from a certain direction is

$$I(\nu) = I_0(\nu) \times (1 - e^{-\tau(\nu)}) \qquad (11)$$

where $I_0(\nu)$ is the intensity of a black body, which is $I_0 = \frac{2\nu^2}{c^2}\,kT$ according to the law of Rayleigh-Jeans. The value of I_0 may be obtained by measuring intensities in optically thick regions, such as the directions $l = 327°.5$ and $l = 45°$. A new discussion of such observations is given by M. SCHMIDT [1]). He finds that I_0 corresponds to a black-body temperature $T = 125$°K, which value has been used throughout. In the absence of continuous background radiation, $I(\nu)$ is the recorded intensity. It has been shown [2]) that continuous radiation of intensity $I_{c,r}$ from sources behind the hydrogen atoms decreases the observed intensity by the amount $I_{c,r}(1 - e^{-\tau(\nu)})$. In that case the optical depth is related to the intensity by the formula

$$\tau = -\ln\{1 - I(\nu)/(I_0 - I_{c,r})\}\,. \qquad (12)$$

In the reductions described in this article, no allowance has been made for this effect. From observations with a continuum receiver at 22 cm wavelength [3]) it was found that the continuous radiation originating in the region $R > 8.2$ kpc, which is studied here, is negligible. Only four of the discrete sources in this region may seriously influence the 21-cm line intensities. The positions of these sources and their intensities observed with the present antenna, are

---

[1]) M. SCHMIDT, *B.A.N.* **13**, 247 (No. 475, fourth paper), 1957.
[2]) *B.A.N.* **12**, 117 (No. 452), 1954. See also J. P. HAGEN, A. E. LILLEY, and E. F. MCCLAIN, *Ap. J.* **122**, 361, 1955.
[3]) G. WESTERHOUT, *B.A.N.* **13**, 105 (No. 472), 1956.

© Astronomical Institutes of The Netherlands • Provided by the NASA Astrophysics Data System

1957BAN....13..201W

Cas A : $l = 79°.5$, $b = -2°.0$, $I = 0.23\ I_0$
Cyg A : $l = 43°.8$, $b = +5°.0$, $I = 0.12\ I_0$
Cyg X : $l = 45°.7$, $b = +1°.6$, $I = 0.07\ I_0$ (uncertain)
Tau A : $l = 152°.3$, $b = -4°.3$, $I = 0.08\ I_0$

None of these positions coincides with the position of one of our profiles, and no corrections have been applied for their absorption effect. If a discrete source would coincide in position with a line profile and no correction would be applied, the density of the hydrogen between the sun and the source would be found too small, provided the absorbing hydrogen clouds do not have a deviating motion. The density behind the source would not be influenced.

6. *Random cloud velocities.*

The radial component of the random velocities of the clouds of a group with respect to their common centre of gravity widens the spectral line.

The distribution of the random cloud velocities may, in principle, be determined from the unpermitted wings of the profiles. In trying to fit gaussian curves to these wings (positive v) in the region $l = 60°$ to $100°$, $b = 0°$ and $\pm 2°.5$, POTTASCH found values of the dispersion σ ranging from 5.8 to 9.7 km/sec, not taking into account the effect of the bandwidth. Similarly, the wings of negative v, at $l = 336°$ to $350°$, $b = 5°.5$ and $-3°.8$, that should be absent because of the high latitude, gave $\sigma = 5.8$ to 7.4 km/sec. These data refer to the velocity distribution near the sun.

Many of the unpermitted wings show extensions of very low intensity reaching as far as 25—40 km/sec from the zero velocity. These may be due to systematic velocity deviations, but may also be part of the distribution function of the random velocities, which could then perhaps be represented by

$$a e^{-v^2/2\sigma^2} + b e^{-|v|/\eta}, \qquad (13)$$

where $b \ll a$ and $\eta \gg \sigma$. It was not found necessary at this stage to investigate this possibility more closely.

An upper limit to σ for more remote parts of the galaxy may be found from the sharpest peaks in the observed profiles. In the directions $l = 185°$ to $210°$ and in several other directions we thus find $\sigma \leq 6.5$ km/sec after correction for bandwidth and conversion into optical depth. The profile at $l = 155°$, i.e., close to the anticentre, gave $\sigma = 5.8$ km/sec. It thus would seem that a gaussian distribution with $\sigma = 6$ km/sec represents the random velocities fairly well. The investigation by POTTASCH also showed that an exponential function of the form suggested by BLAAUW, $e^{-|v|/\eta}$, fits the observational data less well.

The peaks in the line profiles tend to widen slightly with increasing distance to the galactic centre R. As the cloud velocity distribution cannot be separated from widening due to differential galactic rotation in a spiral arm of finite extent, nothing can be said of a variation of velocity dispersion with R.

A discussion of the various methods that may be used to correct the line profiles is given by OLLONGREN and VAN DE HULST [1]). EDDINGTON's approximation for solving the blurring integral is at first sight not applicable, as the width of the dissolving function (the velocity distribution) is of the same order of, or greater than, the width of the non-blurred line profile. Fourier analysis shows, however, that the method may be used with a different coefficient of the second difference. The Fourier transform of the exact resolving function belonging to a gaussian velocity distribution is

$$B(\varphi) = e^{+\varphi^2\sigma^2/2} \qquad (14)$$

The Fourier transform of EDDINGTON's second-order approximation,

$$\tau'(v) = \tau(v) - \varepsilon\Delta^2\tau(v) \qquad (15)$$

is

$$B'(\varphi) = 1 + 2\varepsilon(1 - \cos\varphi\Delta v). \qquad (16)$$

Here, $\Delta^2\tau$ is the second difference of the optical depth and $\varepsilon = c/\Delta v^2$. The velocity interval is $\Delta v = 4.2$ km/sec (= 20 kc/s).

Figure 1 shows the functions (14) and (16) and also the Fourier transform of the exact correction for an exponential velocity distribution, $B(\varphi) = 1 + \eta^2\varphi^2$. It appears that $B'(\varphi)$ with $\varepsilon = 2$ represents fairly well the exact resolving functions with $\sigma = 6$ km/sec or $\eta = 5.5$ km/sec for those parts of the profile where the circular frequency $\varphi = 0.2$ to 0.3. These are the peaks with a sinusoidal shape and peak-to-valley distances of π/φ or 10—15 km/sec. Many of the peaks in the observed profiles have roughly this shape.

If the details in the non-blurred line profile would have been much wider than the velocity distribution, the value $\varepsilon = \sigma^2/2\Delta v^2$ should have been used. With $\sigma = 6$ km/sec we then would have $\varepsilon = 1$.

It was finally decided to correct all profiles with $\varepsilon = 2$, because it was not thought worthwhile, in this large programme, to sort out by detailed analysis regions where slightly different factors might be used.

It may be emphasized that considerable weight in the final choice of ε was given to the practical consideration that the negative ordinates, that may occur after correction, should not be too large. There is no fundamental objection to such values, for it has been shown that, if EDDINGTON's approximation is used to correct for a gaussian blurring function, negative values necessarily occur. But in practice, negative values would have required subsequent smoothing, which would have meant a haphazard way of making the reduction less drastic again.

[1]) *B.A.N.* **13**, 196 (No. 475, second paper), 1957.

© Astronomical Institutes of The Netherlands • Provided by the NASA Astrophysics Data System

1957BAN....13..201W

7. *Thermal motion.*

The kinetic temperature of the neutral hydrogen found from the 21-cm line measurements in regions with a large optical depth is the harmonic mean of the temperatures of the clouds in the line of sight [1]). The temperature found is 125°K. KAHN has shown that collisions of individual clouds may heat these clouds to 3000°K and that this heating mechanism is by far the most important. He also showed that, if the most effective cooling occurs by hydrogen molecules, the cooling to 500°K takes place very rapidly.

SEATON [2]) considered the cooling resulting from excitation by electron impact of low-lying levels in C^+, Si^+ and Fe^+. He found that this mechanism is quite adequate to explain the observed cooling to a harmonic mean temperature of 125° without postulating the existence of H_2 molecules. The electron-ion cooling mechanism is less rapid at higher temperatures than the molecular cooling. SEATON showed that the arithmetic mean temperature with the electron-ion cooling is of the order of 1000°K, while molecular cooling gives a mean temperature of the order of 300°K. Both mechanisms may be active.

In a direction where the optical depth is small we may get on the average equal contributions to the observed intensity from all clouds in the line of sight. Assuming for these clouds an arithmetic mean temperature of 500°K, the velocity dispersion due to thermal motions in the clouds is 2 km/sec. The width between half-intensity points of the 21-cm line emitted by one such cloud is 4.75 km/sec. Some of the widening of the line, so far ascribed to the dispersion in the cloud velocities, must then be caused by thermal motion. If we combine an exponential cloud velocity distribution, for example $e^{-|v|/6}$, with a thermal velocity distribution having a dispersion of 2 km/sec the sharp top of the exponential distribution is cut off and a gaussian curve with a dispersion of 4.5 km/sec fits the top part of the combined cloud-thermal distribution curve quite well down to half the top intensity. Further down the curve has an exponential shape and deviates much more strongly from a gaussian distribution than the original line profiles.

BLAAUW [3]) found an exponential distribution for the velocity distribution of the interstellar calcium clouds. Any influence from thermal motions would pass unnoticed in his material, as *a*) the thermal velocity dispersion for Ca atoms is 4.5 times smaller, and *b*) he only considered the velocities of the separated or nearly separated intensity maxima of individual clouds. It is possible that the top part of the cloud-velocity distribution is indeed more or less exponential. But this would not show at 21 cm if KAHN's theory for the heating of the clouds is correct.

The reduction method described in section 6 corrects for a certain velocity distribution, irrespective of its origin. Therefore, the method will not have to be changed if appreciable thermal motion is present.

It will be very interesting to study in detail the 21-cm absorption lines from discrete radio sources [4]), where owing to the small size of the sources only a few clouds contribute to the absorption. The width of the absorption line of one cloud is determined by the thermal and small-scale turbulent [5]) motions in the cloud. If KAHN's theory is correct, the thermal motion alone would already give these absorption lines halfwidths ranging from 1.5 to 12 km/sec.

8. *Rotation of the Galactic System.*

The average radial velocity of the galactic medium at galactic longitude l, latitude b and distance from the centre R, may be expressed by

$$V_g = R_0\{\omega(R,z) - \omega_0\}\sin(l-l_0)\cos b. \qquad (17)$$

Here, $\omega(R,z)$ is the angular velocity of galactic rotation at a distance R from the centre, and z from the plane. R_0 and ω_0 are the values of R and ω at the sun, and l_0 is the galactic longitude of the centre. For $z = 0$ we have

$$r = R_0\cos(l-l_0) + \sqrt{R^2 - R_0^2\sin^2(l-l_0)}$$

and

$$\frac{dV_g}{dr} = R_0\sin(l-l_0)\Big/\sqrt{R^2 - R_0^2\sin^2(l-l_0)}\cdot\frac{1}{R}\frac{d\omega}{dR}.$$

We may now compute V_g, r and $\frac{dV_g}{dr}$ for a number of fixed values of R. The only data needed are $\omega - \omega_0$ and $\frac{1}{R}\frac{d\omega}{dR}$ for those values of R. We then have a table of r and $\frac{dV_g}{dr}$ (section 10) as a function of V_g. For $z \neq 0$ the formula for $\frac{dV_g}{dr}$ becomes more complicated, but new computations did not appear necessary (see section 10). We have used $l_0 = 327°.5$.

The function $\omega(R,z)$ was computed from a model of the distribution of mass in the Galactic System, given by M. SCHMIDT [6]), which is for a large part based on the observed values of $\omega(R,0)$ for $R < R_0$ [7]).

[1]) F. D. KAHN, Gas Dynamics of Cosmic Clouds, I.A.U. Symposium No. 2, North Holland Publ. Cy., Amsterdam, 1955.
[2]) M. J. SEATON, *Ann. d'Ap.* **18**, 188, 1955.
[3]) *B.A.N.* **11**, 459 (No. 436), 1952.
[4]) J. P. HAGEN, A. E. LILLEY and E. F. MCCLAIN, *Ap. J.* **122**, 361, 1955. See also Radio Astronomy Symposium 1955, I.A.U. Symposium No. 4, Cambridge University Press, 1957.
[5]) L. SPITZER JR and A. SKUMANICH, *Ap. J.* **116**, 452, 1952.
[6]) *B.A.N.* **13**, 15 (No. 468), 1956.
[7]) K. K. KWEE, C. A. MULLER and G. WESTERHOUT, *B.A.N.* **12**, 211 (No. 458), 1954.

© Astronomical Institutes of The Netherlands • Provided by the NASA Astrophysics Data System

1957BAN....13..201W

TABLE 1

Values of $-\{\omega(R,z)-\omega_0\}$ used in the reductions. $\omega_0 = 26.4$ km/sec. kpc. For comparison, R' $(z = 0)$ is given for SCHMIDT's final model.

R	$z = 0$	$z = 0.3$	$z = 0.6$	$z = 0.9$	$z = 1.2$	$z = 1.5$	R'
	$-(\omega-\omega_0)$	$-(\omega-\omega_0)$	$-(\omega-\omega_0)$	$-(\omega-\omega_0)$	$-(\omega-\omega_0)$	$-(\omega-\omega_0)$	$(z=0)$
kpc	km/sec. kpc						kpc
8.2	0	0.16	0.52	0.99	1.49		8.20
8.3	0.48	0.64	0.98	1.42	1.90		8.30
8.4	0.92	1.08	1.41	1.82	2.28		8.39
8.6	1.80	1.94	2.23	2.60	3.02		8.59
8.8	2.63	2.75	3.00	3.34	3.73		8.77
9.0	3.39	3.50	3.73	4.05	4.42		8.94
9.5	5.11	5.21	5.41	5.67	5.99		9.42
10.0	6.56	6.65	6.82	7.03	7.29	7.56	9.88
10.5	7.87	7.96	8.10	8.30	8.54	8.79	10.36
11.0	8.99	9.08	9.20	9.39	9.61	9.83	10.78
11.5	10.07	10.15	10.27	10.43	10.63	10.83	11.19
12.0	10.94	11.02	11.12	11.26	11.44	11.59	11.59
13.0	12.57	12.64	12.73	12.83	12.98	13.12	12.46
14.0	13.94	14.00	14.07	14.15	14.27	14.40	13.33
15.0	15.14	15.20	15.27	15.34	15.43	15.53	14.12
16.0	16.22	16.28	16.34	16.40	16.46	16.52	14.89

When our reductions had reached the stage where values of $\omega(R)$ were needed, only model no. 2 of SCHMIDT was available. The values given in Table 1 and used in our reductions refer to this model, and differ from the values that may be computed from his final model. For comparison we have added to the table those values of R, at which the given $\omega(R)$ for $z = 0$ is reached in SCHMIDT's final model. It may be seen that R comes out smaller in the final model. If our figures of the hydrogen distribution in the plane and perpendicular to it are to be compared to the final model, allowance should be made for this difference; roughly, the scale of the regions $R > 8.2$ kpc should be multiplied by a factor 0.9. In Table 2, some values r' that with SCHMIDT's final model would

TABLE 2

Values of r' in kpc, based on SCHMIDT's final model for various values of r used in this investigation.

$l =$ / r	345° r'	5° r'	35° r'	65° r'	80° r'	110° r'	130° r'
2	2.00	2.00	2.00	1.89	1.88	1.87	1.86
4	4.00	4.00	4.00	3.84	3.76	3.62	3.57
6	6.00	6.00	6.00	5.78	5.50	5.31	5.27
9	9.00	9.00	8.85	8.24	8.07		
12	12.00	12.00	11.56				
15	15.00	14.87	14.16				
20	19.49	19.19					

correspond to the r used in our reductions, are given. In SCHMIDT's final model the mass distribution of model 2 is adjusted so that the values of the rotational velocities for $R < 8.2$ kpc are equal to the observed values. From the present data we cannot decide from which model we should have taken the rotational velocities in the outer parts of the Galactic System. Table 2 therefore illustrates the uncertainty in the distance scale.

For each longitude observed a graph has been prepared, giving the distance to the sun, r, as a function of radial velocity or frequency-displacement in the line for $b = 0°$, 5° and 10° (example in Figure 4g).

9. *Deviations from circular motion.*

The conversion of radial velocity into distance from the sun is based on the assumption of circular motion around the galactic centre. The only deviations for which corrections have been applied, are the random velocities relative to the local centres of gravity. From the line profiles, it is clear that this assumption fails in several regions in the neighbourhood of the sun. In the profiles for $l = 57°.5$ and $l = 60°$ for example, where no positive radial velocities should occur, some of the tops are situated between + 3 and + 5 km/sec, indicating a systematic motion of a group of clouds deviating from the circular motion. A very striking case is presented in the plots of optical depth against radial velocity in the anti-centre region (Figure 8), where maxima occur with velocities up to − 30 km/sec and + 25 km/sec. We shall come back in detail to this region in section 14c. Such group motions can be detected only in the neighbourhood of the sun. Regions farther away provide no ways of detection and therefore must have an uncertainty in the positions of the maxima of hydrogen density which may be of the

© Astronomical Institutes of The Netherlands • Provided by the NASA Astrophysics Data System

1957BAN...13..201W

order of 0.5 to 1.5 kpc in regions away from the centre and anti-centre. In section 14e we point out some cases where velocity deviations are suspected.

10. *Conversion of optical depth into density.*

It has been shown in *B.A.N.* No 452 that the number of hydrogen atoms per unit velocity interval in the absence of random motions, $\mathfrak{N}(V)$, is related to the temperature and the corrected optical depth by the formula

$$\mathfrak{N}(V) = 1.835 \times 10^{13}\, T\tau'(v). \qquad (18)$$

After correction for random velocities, a part of a spiral arm of certain dimensions does not give an infinitely narrow profile, but a profile widened by internal differential motions due to differential galactic rotation. The hydrogen density may be found from

$$n_H(r) = \mathfrak{N}(V)\, dV_g/dr, \qquad (19)$$

where $\frac{dV_g}{dr}$ is the widening factor.

From the optical depth $\tau'(v)$, corrected for cloud velocities according to section 6, the density as a function of radial velocity may be obtained with

$$n_H(r) = 0.0744\, \tau'(V_g)\, dV_g/dr, \qquad (20)$$

taking $T = 125°$K and expressing $\frac{dV_g}{dr}$ in km/sec. kpc.

It is quite probable that there are many local temperature deviations. It will be shown in section 12 that the adoption of a constant temperature $T = 125°$K throughout introduces serious errors in the computation of n_H in such regions.

With the relation between V_g and r we may now compute $\frac{dV_g}{dr}$ and $n_H(r)$. While V_g has been computed for three different latitudes, $\frac{dV_g}{dr}$ was only computed for $b = 0°$; using this same value for $b = 10°$ introduces errors up to 10% in n_H, which are smaller than the estimated uncertainty in τ'. The computation of V_g and $\frac{dV_g}{dr}$ has to be made only for one quadrant, from $l = 57°.5$ to $l = 147°.5$. In the quadrant $l = 327°.5$ to $l = 57°.5$, the relation between V_g and r is the same except for a term in r (= the length of the line of sight in the region $R < 8.2$ kpc).

PART II

DETERMINATION OF THE HYDROGEN DENSITY

11. *The reduction procedure.*

a. The mean curves from the catalogue were tabulated twice at 20 kc/s intervals, one table being shifted 10 kc/s with respect to the other. This has the advantage that the results of one table form a check on those of the other, and that the reduced curves can be drawn smoothly. All computational checks were made by plotting the reduced curves with the unreduced; any mistake showed up immediately as an irregularity in the curve. The ordinates were read off in mm; the height of the main top at $l = 50°$, which was assumed to have a top intensity $I = 100°$K, was 129 mm. A correction for bandwidth was applied by eq. (2). The value of $h' = h - 0.3\,\Delta^2 h$ was found easily by taking three successive numbers h_{-1}, h and h_{+1} and calculating their sum $h' = -0.3\, h_{-1} + 1.6\, h - 0.3\, h_{+1}$ with a desk computer.

b. At 40 kc/s intervals, the values of h' were taken from the set of tables for $b = +10°$ to $b = -10°$ for any one longitude, and plotted as a function of b. Smooth curves were drawn through these points. They represent cross sections perpendicular to the galactic plane at one frequency. The curves were tabulated and the correction for antenna pattern was applied as described in section 4.

From the angle between the galactic equator and the vertical, the effective halfwidth of the antenna pattern perpendicular to the equator, A, at the approximate time of observation, was determined. The latitude interval Δb was taken $1°.25$, in order to obtain a smooth corrected curve. From this, $\varepsilon_A = 0.058\, A^2$. Figure 3 gives an example of the result of this correction.

FIGURE 3

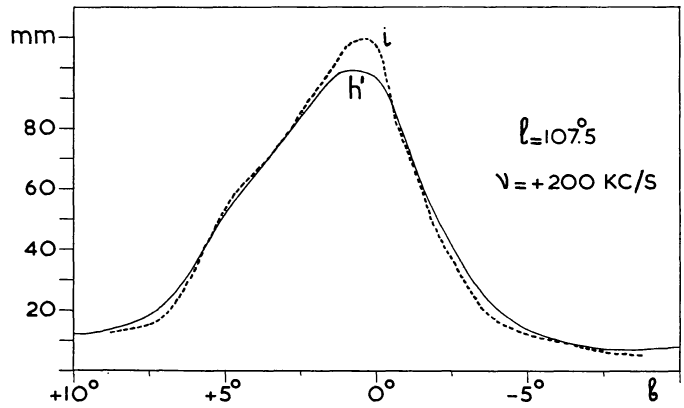

Example of the correction for antenna pattern.

c. The values of i/h' were plotted against frequency for each profile, smooth curves drawn through the points, and the correction factors i/h' were read for intermediate frequencies and used to correct the tabulated profiles.

d. The corrected values i were converted into optical depths by means of the tabulated function $\tau = -\ln(1 - i/162)$ where 162 is the equivalent in mm of the intensity at infinite optical depth, $I_\infty = 125°$K.

© Astronomical Institutes of The Netherlands • Provided by the NASA Astrophysics Data System

1957BAN....13..201W

e. The optical depths were corrected for cloud velocities by taking three successive numbers τ_{-1}, τ and τ_{+1} and computing the sum $\tau' = -2\tau_{-1} + 5\tau - 2\tau_{+1}$, which corresponds to $\tau' = \tau - 2\,\Delta^2\tau$.

f. The values of τ' were plotted against frequency, and the curves were compared very carefully with the original line profiles. The correction methods tend to enlarge strongly any computational or reading errors. It appeared that at many instances, when the original profiles $h(\nu)$ were read to 0.5 mm, an accuracy far better than the absolute accuracy, a number of spurious wiggles, 20 kc/s wide occurred in the τ' curves, because the tabulated h curves were not smooth enough. It was only slightly more work to read the curves to 0.1 mm, by which the wiggles completely disappeared. Of course, one may also draw a mean curve through the wiggles, but the other method proved easier. Great care was taken that remnants of all peaks, valleys or wiggles in the τ' curves were detectable in the original line profiles. This method proved very successful in detecting even small reading, computational or drawing errors. In several cases, when comparison with neighbouring profiles showed an extreme deviation, all operations, from the drawing of zero lines and smoothing of the measured profiles, were rechecked.

g. Negative values of τ' occur in the corrected profiles, particularly where a rather high and narrow top is present near the zero velocity. Tests made by CASPARIE on artificial line profiles showed that if the velocity distribution resembles a gaussian function, the correction method used gives increasingly negative values with increasing slope, i.e. for narrower profiles. It was found that the best method to correct for negative optical depths is to distribute their sum evenly over the points of the adjacent positive slope, and not to change the top value. For consistency, a similar correction should be applied when a second maximum or a high part of the profile closely follows the first maximum, even though in such a case no negative values are reached. This is generally the case at velocities away from the zero velocity. No attempt has been made to correct such values of τ', except in extreme cases where a very deep valley was obviously caused by this correction error. Therefore, particularly near points of high hydrogen density, it is possible that inter-arm densities are found too low. It is hoped that in future reductions such difficulties can be overcome by applying more exact correction methods. Such methods will have to make use of electronic computing machines, using successive approximations. Every single profile, or each set of profiles for a certain region may then be analyzed more fully and perhaps allowance can be made for different velocity distributions and temperatures. As the correction for negative τ' was only necessary very close to the zero frequency, it did not influence the final density contours, where the region close to the sun has been omitted.

h. The hydrogen densities may now be determined. As the relation (20) may be used for all profiles at one l and different b, it was found worth while to compute for each longitude the function

$$\tau'(V_g) = \frac{n_H(r)}{0.0744\, dV_g/dr}$$

for values of $n_H(r)$ ranging from 0.05 to 1.6 atoms/cm^3. This function was plotted on transparent graph paper, on the same scale as the τ' curves. Also on this scale, in the same graphs, the function

$$V_g(\text{kc/s}) = -4.735\, R_\circ \{\omega(R,z) - \omega_\circ\} \sin(l - l_\circ) \cos b$$

as a function of r was plotted for $b = 0°$, $5°$ and $10°$ (Figure 4g). The graphs had to be made for the quadrant $l = 57°.5$ to $l = 147°.5$ only; in the other quadrants, they were reversed, while between $l = 327°.5$ and $l = 57°.5$ a constant term was added to r. By putting such a graph on top of the τ' curves, the distance r from the sun may be read immediately for points where $n_H = 0.05$, 0.1 .... 1.6 atoms/cm^3. At each longitude these points were drawn on graph paper as a function of latitude and distance from the sun.

Finally, by connecting corresponding points we constructed equidensity curves in planes through the sun, perpendicular to the galactic plane. The consecutive steps of the reduction procedure are illustrated by Figure 4, while the density contours are given in Figure 9.

12. *Accuracy of the density contours.*

It is very difficult, in view of the successive approximations, to determine the accuracy of the final density contours. Various tests, namely, a comparison of different reduction methods, the use of artificial line profiles and a comparison with other observations indicate the following accuracies:

intensity	h	5%
correction for bandwidth	h'	5%
correction for antenna pattern	i	5%
correction for cloud velocities	τ'	10%

The estimated accuracy in the densities is therefore of the order of 15%, due to errors in the measurements and the correction methods. An additional error, which may rise to 10%, is introduced by taking for the factor $\frac{dV_g}{dr}$ for profiles with $b \neq 0°$ the value used for $b = 0°$.

© Astronomical Institutes of The Netherlands • Provided by the NASA Astrophysics Data System

1957BAN....13..211W

FIGURE 4

Example of the various operations applied to a line profile

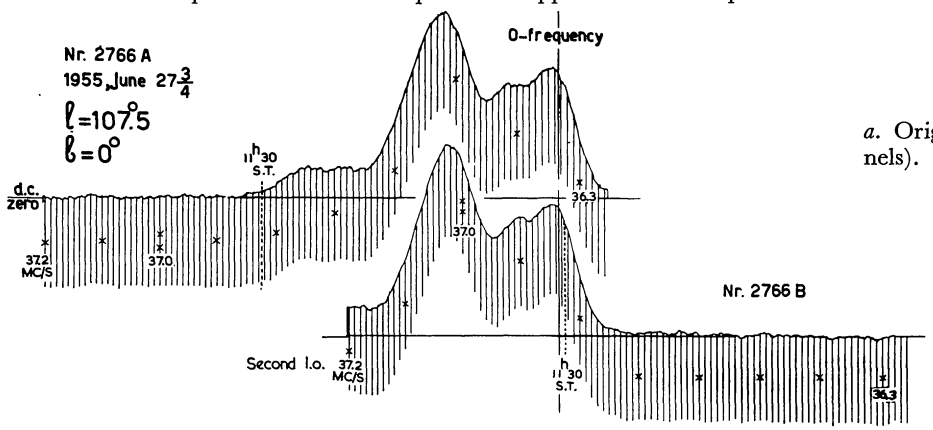

a

a. Original record (2 channels).

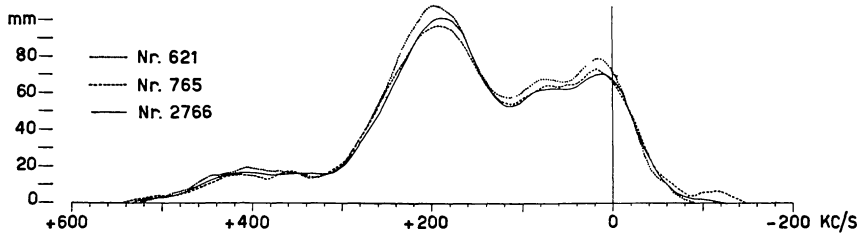

b

b. Three profiles, corrected to the same intensity scale.

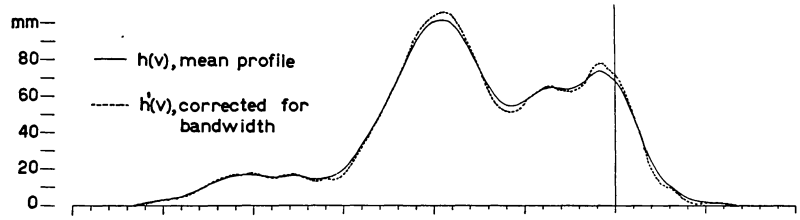

c

c. Mean profile and correction for bandwidth.

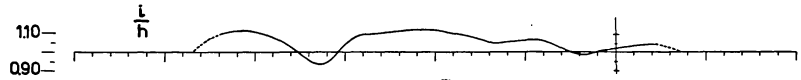

d

d. Correction factor for antenna pattern.

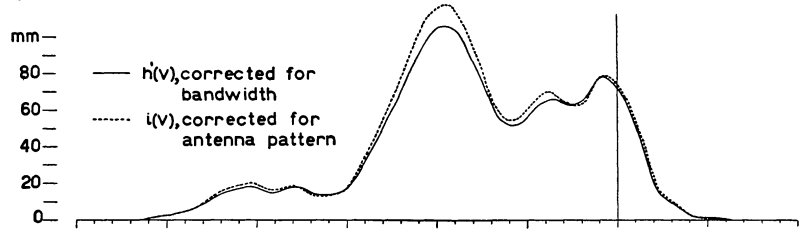

e

e. Correction for antenna pattern.

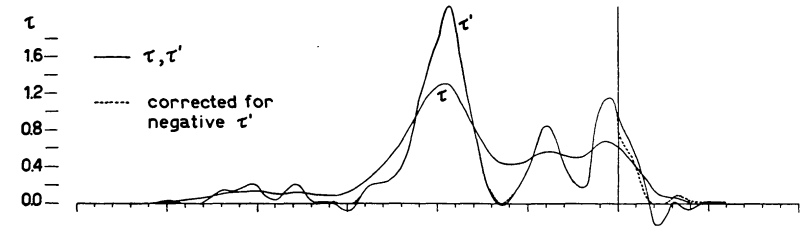

f

f. Conversion in τ and correction for cloud velocities.

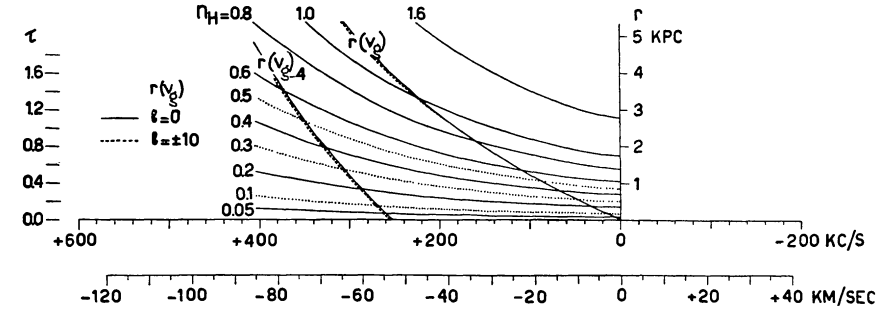

g

g. τ' as a function of n_H and V_g, and r as a function of V_g. In the reductions, this graph was plotted on transparent paper and put on top of the τ' curve in *f* to read off $n_H(r)$.

© Astronomical Institutes of The Netherlands • Provided by the NASA Astrophysics Data System

1957BAN...13..201W

In the conversion of intensity into optical depth, the value of $I_0 = 125°K$ has been used in every position. It has been suggested [1]) that this temperature is not the same at every point in the Galactic System. From the observations it is clear, however, that in the neighbourhood of the sun there are no large regions with systematically different temperatures. The region around $l = 42°.5$, the centre and the anti-centre directions give equal values for the harmonic mean temperature, I_0. Regions farther away from the sun than about 2 or 3 kpc do not contribute much to this temperature. In other parts of the Galactic System the temperature cannot be determined with any certainty. It is not unlikely, however, that at least at a distance to the centre, roughly equal to that of the sun to the centre, conditions are the same. We have therefore assumed that I_0 is the same in the parts of the Galactic System discussed here. If the line of sight passes through regions of different temperature, which together provide the harmonic mean temperature, it is next to impossible to separate them. It is quite probable that in many local regions in the various spiral arms the temperatures differ considerably from the adopted $I_0 = 125°$, and consequently the optical depths and densities may be in error, in places, by over 50%. Suppose, for example, that for a normal maximum somewhere in a 21-cm line, the local $I_0 = 80°K$. With a maximum $I = 50°K$ we then have $\tau = 0.981$. A reasonable value for τ' is 2.25, which gives $n_H = 0.107 \frac{dV_g}{dr}$. If we had taken $I_0 = 125°K$, we would have found $\tau = 0.511$, $\tau' = 1.05$ and $n_H = 0.078 \frac{dV_g}{dr}$, i.e. 1.4 times too small.

The neglect to take differences in temperature into account may also influence the width of a spiral arm in radial direction. If in a certain region the temperature is higher than 125°K, and we apply the standard correction, the width of a maximum in a line profile comes out larger for low values of τ, than it should be if the correct I_0 had been used. The halfwidth, however, does not change appreciably. Tests showed that this may easily give an apparent widening of the low-intensity wings of a spiral arm of 40%, if the temperature there is 200°K instead of the 125°K used.

A similar effect appears if the dispersion in the cloud velocities at a certain position is different from the adopted dispersion. A line profile from a region where the dispersion is 9 km/sec will be undercorrected if our standard method (6 km/sec) is applied. The maximum optical depth will be found too low. The area under the curve, however, should remain the same (total number of atoms). Therefore, at a low level a widening will be found, which for the case mentioned above is of the order of 10%. At most longitudes a widening of 40% will not be very noticeable. At $l = 65°$, $r = 3$ kpc, for example, a width of 8 km/sec in the line profile corresponds to 600 pc. An increase by 40% means 240 pc in radial direction. Close to the anti-centre, however, the effect becomes more important. At $l = 120°$, $r = 3$ kpc, the same line width corresponds to 1200 pc and a 40% increase there means 480 pc.

If too small a correction factor, or too low a temperature is used in these regions, the density maxima tend to widen considerably in a radial direction. This shows in several places in plate B (opposite p. 247) as elongated features extending towards and away from the sun.

It has already been pointed out in section 9 that group motions deviating from the adopted circular motion will shift density maxima by amounts which may well be of the order of 0.5 to 1.5 kpc.

In the future it may be possible to make an estimate of the variation in random velocities and temperature, and to find some indication of systematic motions from detailed comparisons of different regions in the galaxy. It should be realized that such deviations only show up in investigations like the present one, where large regions may be intercompared.

Details considerably smaller than the half-power widths of the instrument cannot be distinguished. In the tangential direction, these are given by the antenna pattern, which is $1°.9 \times 2°.7$. In radial direction the bandwidth of 37 kc/s is the determining factor. For a given point, these widths may be expressed in linear dimensions. On the assumption that details smaller than $\frac{1}{2}$ halfwidth become invisible, we have computed Table 3, where the dimensions of the smallest detectable individual hydrogen regions are given for various points.

A smaller bandwidth would show up smaller details in the radial direction, but the position of the hydrogen clouds causing these details would be indeterminate for two reasons. The random cloud velocity would give an uncertainty of at least 6 km/sec and systematic velocity deviations give an uncertainty of about the same order. For a large-scale survey like the present one the bandwidth used is therefore quite suitable.

13. *Variations in the reduction methods.*

a. When the reductions were started, no corrections were applied for the bandwidth of the receiver. It was not until we received a Harvard interim report [2]) in which an original record of the profile at $l = 110°$, $b = 0°$ appeared, that we realized its importance.

[1]) D. S. Heeschen, *Ap. J.* **121**, 569, 1955; R. D. Davies, *private communication.*

[2]) Th. A. Matthews, mimeographed paper, Meeting A.S.P. and A.A.A.S., Dec. 1954.

© Astronomical Institutes of The Netherlands • Provided by the NASA Astrophysics Data System

1957BAN....13..201W

TABLE 3

Smallest detectable regions in tangential and radial direction, on the assumption that 1/2 halfwidth can still be detected.

l	r = 1 kpc			r = 4 kpc			r = 8 kpc			r = 12 kpc			r = 16 kpc		
	tang.		rad.	tang.		rad.	tang.		rad.	tang.		rad.	tang.		rad.
	pc	pc	pc	pc	pc	pc	pc	pc	pc	pc	pc	pc	pc	pc	pc
345	24	17	320	94	66	210	189	133	—	283	199	210	377	265	380
5	24	17	210	94	66	270	189	133	410	283	199	210	377	265	370
30	24	17	320	94	66	—	189	133	230	283	199	320	377	265	490
60	24	17	590	94	66	290	189	133	350	283	199	490	377	265	—
205 90	24	17	230	94	66	320	189	133	510	283	199	—	377	265	—
165 130	24	17	450	94	66	900	189	133	1550	283	199	—	377	265	—

The Harvard profile, obtained with a 15 kc/s bandwidth, has deeper minima and sharper maxima than the Leiden profile. When smoothed over a 37 kc/s bandwidth it was almost identical to the Leiden one.

At that time all corrections except that for bandwidth had been applied to about one third of the profiles. A method had to be found to apply the latter correction afterwards, rather than to repeat all computations. The successive operations, as enumerated in section 11, are B (bandwidth), A (antenna pattern), τ (optical depth), and C (cloud velocities).

The correct order of reduction is BAτC. The profiles had been corrected by means of the method AτC. It was shown theoretically and in practical examples that the operation BAτ may be inverted to AτB if slopes in the observed profiles are not steep. This also holds for high tops, where the operation τ yields very much steeper slopes and relatively much higher maxima than in the observed profiles. From tests on some profiles in which conditions are rather extreme, such as $l = 50°$ and $l = 147°.5$, it appeared that the differences between methods AτB and BAτ reach a maximum of about 10% in the values of τ.

It may easily be shown that the operations BC and CB are identical. Therefore, if errors of the order of 10% are permissible, the reduction method AτCB may be used instead of BAτC. Consequently, in all computations that had been made up to that moment, the bandwidth correction was applied after the cloud-velocity corrections.

An example of the differences between the two methods for $l = 65°$, $b = 0°$ is given in Figure 5. The Leiden profile at $l = 110°$, $b = 0°$, corrected in this way, is almost identical to the Harvard profile, not corrected for bandwidth, but otherwise with the same constants.

b. In the region $l = 340°$ to $l = 42°.5$, where the line profiles were not measured in points along lines perpendicular to the galactic equator, but in points

FIGURE 5

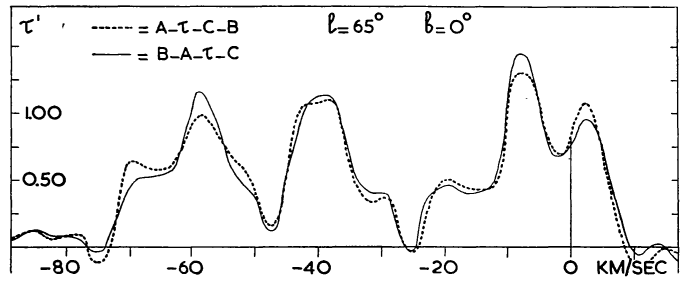

Comparison of the correct (B A τ C) and alternative (A τ C B) correction methods.

along declination circles (Table 1 of the first article of this series, p. 159), all profiles were reduced to curves of τ' by the standard method. In correcting each set of profiles for the antenna pattern, no allowance was made for the difference in longitude of adjacent profiles. This is permissible because the difference is of the order of 1°.2, smaller than the width of the antenna pattern and the 2° latitude interval. Also, the structural changes in longitude are much slower than those in latitude. Cross sections, based on the τ'-curves, would have been planes making a certain angle with the galactic plane, and positionally difficult to interpret. Therefore, at each latitude τ' was plotted against l at 10 kc/s frequency intervals. About 50 curves per latitude were made. From the curves, values of τ' were interpolated at $l = 340°$, 342°.5, ... 42°.5, thus giving new τ'-curves, from which the density cross sections in planes perpendicular to the galactic plane were made in the manner described in section 11h.

c. The profiles in the region $l = 120°$ to $l = 220°$ also were taken at points that do not precisely form a regular array. As the differences were small (Table 2 in the first article of this series, p. 160), all reductions were applied as though the profiles were situated along lines perpendicular to the galactic plane.

© Astronomical Institutes of The Netherlands • Provided by the NASA Astrophysics Data System

1957BAN....13..201W

PART III

RESULTS

14. *Interpretation and discussion.*

a. The cross sections on pages 223 to 246 (Figure 9) give a detailed picture of the density distribution. It is difficult to obtain from these cross sections an impression of the Galactic System as a whole. In Leiden this was done by copying the most important features of the cross sections on colourless „Perspex" sheets. These were combined in a fan-shaped pattern with the sun as centre by mounting them vertically on to a perspex plate. The advantage of such a three-dimensional model is obvious. The spiral arms may be traced in space, while interconnections between arms and irregularities in the latitude distribution are easily discernable.

From a careful study of this model and of the individual cross sections, plate A (opposite page 246) was prepared, in which the hydrogen distribution is represented as seen from the north galactic pole. It should be realized that in such a picture it is difficult to give accurate density gradients. Moreover, arms like the faint outer arm between $l = 12°.5$ and $l = 30°$, are shown as separate arms, although the minima between the arms in many cases are very shallow. We have attempted to display in this picture every detail concerning position and interconnection of arms, rather than to give accurate densities. Therefore no density ratios should be estimated from this figure. The arms in the region $R < 8.2$ kps have been taken from the following article by M. SCHMIDT. SCHMIDT gives only the maximum hydrogen densities in planes perpendicular to the galactic plane and projected on this plane. To provide a picture consistent with his map, the maximum hydrogen densities in the z-direction were determined from the cross sections and projected on the galactic plane. Density contours were drawn through the points thus obtained (plate B, opposite page 247). In several instances arms that are clearly separated in the cross sections, because they are situated at different heights above the plane, overlap in such a projection, for example at $l = 190°$, $R = 12$ kpc.

b. A striking feature of many cross sections is the tilt of the arms with respect to the galactic plane. In the region $l = 55°$ to $125°$ this tilt averages approximately $+ 1°.5$ and is opposite to the tilt found in the central parts. Most of it is due to the fact that the standard galactic plane does not coincide with the correct galactic plane. In section 16 a preliminary determination of the true galactic plane is made. In a number of places, real deviations from the mean plane exist, for example near $l = 80°$, $r = 3$ kpc and in the arms at $l = 75°$, $r = 3.5$ kpc and $l = 190°$, $r = 4$ kpc.

c. The cross sections near $l = 340°$ and between $l = 130°$ and $l = 165°$ show very little detail. The velocity-distance relation in those regions is so steep that the bandwidth and the cloud-velocity dispersion wipe out all details. At $l = 135°$, $r = 4$ kpc, for example, the 6 km/sec cloud-velocity dispersion corresponds to 2 kpc in radial direction. Also, deviations from circular motion show up as very large distance deviations, while, as has been explained in section 12, a wrong correction for cloud velocities might also give considerable distortions. Therefore, in the region $l = 135° - 160°$ reliable cross sections cannot be made. The available line profiles, corrected for cloud velocities, were plotted in Figure 8 against latitude and radial velocity in the form of curves of equal optical depth. The high optical depths reached in this region depend strongly on the adopted hydrogen temperature. If the temperature would have been taken 126°K instead of 125°K, optical depth 5.0 would have become 4.0. This also shows that the temperature determined from these profiles cannot be very far off. The absolute value of I_0 of course depends wholly on the assumed $I = 100$°K for the main top at $l = 50°$, $b = 0°$, a value which has an uncertainty of 20% [1]). From the position of the central maximum in the longitudes 135° to 160° the position of the anti-centre may be determined within 0°.5. If we assume that the deviations of circular motion cancel along the line of sight, we find $l = 148°.5 \pm 0°.5$. It is very difficult to estimate how large a systematic error comes into this determination. The mean distance of the hydrogen emitting the central maximum is about $r = 1.5$ kpc. If the spiral arms are circular in this part of the galaxy, the first two arms outside the sun would pass at distances of 0.2 and 2.2 kpc. Probably the maximum is a blend of the profiles of the hydrogen in both arms.

It is interesting to note the fairly large deviations from circular motion showing up in Figure 8. As an example of what sort of deviations one might expect in other parts of the Galactic System let us follow the secondary maximum at $l = 150°$, $b = 0°$, $V = - 11$ km/sec. At $l = 145°$ it has a velocity of $- 15$ km/sec. At $l = 135°$ it is still visible at $- 20$ km/sec. Assuming circular motion, we have placed it in the cross section $l = 135°$ at $r = 4.5$ kpc; it may be traced down to $l = 120°$, at which longitude it appears to merge into the main Perseus arm at $r = 3$ kpc. If our very tentative assumption that this is still the same density maximum is correct, and that as a whole it has a deviating velocity, we may infer from Figure 8 ($l = 145° - 150°$) that this velocity is $- 13$ km/sec. This means, that for example at $l = 130°$, the maximum should not be placed at $r = 3.6$ kpc,

[1]) C. A. MULLER and G. WESTERHOUT, *B.A.N.* **13**, 151 (No. 475, first paper), section 4, 1957.

© Astronomical Institutes of The Netherlands • Provided by the NASA Astrophysics Data System

1957AN....13..201W

but at $r = 1.4$ kpc. The connection of the maxima over this range is very uncertain, but shows how large some errors may become, particularly in the anti-centre region.

d. In all cross sections the region near the sun has been left blank. It is impossible to assign any position to the hydrogen causing the main top of the line profiles. Small deviations from circular motion may easily displace the maximum over 200 parsec, and bandwidth and cloud velocities likewise prevent greater accuracy. An investigation into the hydrogen distribution for $r < 500$ parsec should be made from plots like those in the anti-centre region (Figure 8), where the lines of sight are made parallel. Preferably also line profiles at still higher latitudes should be available. Similar plots, giving antenna temperatures and extending to about $b = \pm 30°$, have been made for several longitudes by H. L. HELFER and H. E. TATEL [1]).

A very tentative determination of the mean hydrogen density in the neighbourhood of the sun has been made. Mean values of τ' in the maxima near the zero velocity were determined for large regions at different latitudes. The distance of the hydrogen to which these mean optical depths refer has been arbitrarily taken as 100 parsec. Formula (20) then gave $\bar{n}_H$, using the value of $\frac{dV_g}{dr}$ for $r = 100$ pc. The results for the region $l > 60°$ are presented in Table 4a.
In the region $l < 57°.5$, the lines of sight pass through the central parts of the galactic system, which up to $l = 40°$ are treated separately by M. SCHMIDT in the following article. It is very difficult to decide which part of the profile near zero velocity in this region is due to nearby hydrogen. Only upper limits of the mean density could be given. SCHMIDT separated the contributions from near and far points for $r > 200$ pc, and from his data n_H for $200 < r < 300$ pc has been determined. These are given in Table 4b.

TABLE 4

Mean hydrogen densities in the neighbourhood of the sun.

a

l ($r < 200$)	$b = +7°.5$ $\bar{n}_H$	$0°$ $\bar{n}_H$	$-7°.5$ $\bar{n}_H$
210°	.35	.17	.09
195	.59	.75	.29
180	.13	.09	.10
165	.21	.08	.02
130	.66	.57	.15
115	.76	1.22	1.09
100	.99	1.27	.93
85	.73	.92	.79
70	.63	.79	.47

b

l ($b \approx -1°.5$)	$200 < r < 300$ $\bar{n}_H$	$r < 200$ $\bar{n}_H$
30°	.99	<.4
20	.92	<.8
10	1.17	<.9
0	.90	
355		1.3 ?
350	.76	
345		1.1 ?

The reductions for the present article were started on the circle around the galactic centre where the radial velocity $V_g = 0$. This circle is the circle $R = 8.2$ kpc for $b = 0°$, but has a smaller radius for $b \neq 0°$, due to the decrease of the circular velocity with increasing z.

The intensity near zero velocity is determined by hydrogen in the vicinity of the sun as well as by distant hydrogen. This gives rise to an apparent increase of the densities, particularly at the higher latitudes, where the density in the far parts is negligible. No attempt was made to separate the two contributions. In general, in the region $l < 57°.5$, the part of the cross sections for $R < 8.3$ kpc should not be considered to represent the correct density distribution for the values of r indicated. In some instances this limiting value of R has to be increased (e.g. at $l = 352°.5$) or may be diminished (e.g. at $l = 25°$, where hardly any contribution from hydrogen close to the sun seems to be present).

e. The region $l = 40°.9$ to $l = 57°.5$, $R < 8.2$ kpc has not been treated by SCHMIDT. In this region it is extremely difficult to decide which part of the very high optical depths is due to nearby hydrogen. A very tentative separation of near and far contributions has been made after a study of contour lines of optical depth in a velocity-latitude system, such as Figure 8. It was found that a maximum occurs between $l = 65°$ and $l = 42°.5$. $b = -2°.5$, $V_g = +5$ to $+10$ km/sec. This maximum is probably due to hydrogen near the sun. A very high maximum with τ' between 3 and 6 is situated between $l = 52°.5$ and $l = 47°.5$. At $l = 42°.5$ it has $V_g = +5$ km/sec, at $l = 47°.5$ it has $V_g = 0$ km/sec. We tentatively assume that this maximum must be due to hydrogen between $r = 3$ and $r = 4$ kpc. The contour lines in this region are drawn in plate B according to this assumption, and therefore their position is very uncertain. The region is indicated by thick lines.

[1]) *Ap. J.* **121**, 585, 1955.

© Astronomical Institutes of The Netherlands • Provided by the NASA Astrophysics Data System

1957BAN....13..201W

f. At many places in the cross sections, density contours have been interconnected rather arbitrarily. Therefore, at some places strangely shaped extensions stick out of the main bodies of the arms. In view of the limited resolving power of the instrument, it was not thought proper to create too many "individual cloud groups" of sizes smaller than 200 pc. Many of these extensions, as well as some branches of the arms, may possibly be explained by assuming that they are due to deviations from circular motion of a group of clouds or part of an arm.

At $l = 125°$, $r = 2.5$ kpc, $z = +200$ pc, it is quite possible that the trunk sticking out from the Perseus arm would have to be placed at $r = 3.5$ kps, its displacement being caused by a velocity deviation of $+6.5$ km/sec.

The complicated situation at $l = 42°.5$, $R = 9.5$ to 11 kpc (plate A) may be due to systematic deviations from the circular velocity of the order of 2.5 km/sec of a large part of the arm. The same applies to the split in the Perseus arm around $l = 37°.5$, $R = 10.5$ kpc.

It seems impossible at the present time to find means to determine such deviations with any certainty.

15. *Description of the spiral arms.*

We shall now proceed with a description of the main features of the spiral arms in the region $R > 8.2$ kps. A discussion of the arms inside this circle may be found in the following article on p. 261.

a. The *Orion arm* may be followed from $l = 340°$ to $l = 220°$. Between $l = 40°$ and $l = 55°$ the position of the arm is difficult to determine. We assume tentatively that between $l = 40°$ and $l = 50°$ the main body of the arm lies just inside the circle $R = 8.2$ kpc, at a distance of about $3 - 4$ kpc from the sun. Over the whole region between $l = 55°$ and $l = 100°$ the position of the main body of the arm must be very close to the sun, but cannot be determined, as its velocity is near the zero velocity. A branch gradually moves outward, starting at $l = 45°$, lying at a mean distance $R = 8.5$ kpc between $l = 52°.5$ and $l = 65°$. Between $l = 65°$ and $l = 72°.5$ this branch turns sharply outward to $R = 8.9$ kpc and stops there. At $l = 80°$ the arm splits up again and a very dense part runs about 100 pc above the plane at $R = 8.6$ kpc. The rest of the arm joins this branch at $l = 105°$. From the profiles for $l > 150°$ it is clear that the sun is situated at the inner edge of the arm. From $l = 170°$ onwards the mean distance of the arm is between $R = 8.7$ and 9 kpc.

b. The *Perseus arm* obtained its name from the massive association around the double cluster in Perseus. However, at the position of this cluster, $l = 102°.8$, $b = -2°.9$, $r = 1.3$ kpc, we find a density minimum. The arm may be followed from $l = 340°$ to $l = 220°$. Between $l = 340°$ and $l = 15°$ it is split up in two parts. The innermost runs at $R = 9$ kpc, $z = -400$ pc, the outer at approximately $z = -200$ pc to $l = 0°$, and from there on moving to about $z = +200$ pc at $R = 11.5$ kpc. At $l = 15°$ both parts come together at $R = 10.5$ kpc, $z = 0$ pc. From there onwards it is rather complicated, with several high-density regions at different heights, but remaining at a mean height of 0 pc and a distance between $R = 10.5$ kpc and 11 kpc except for a branch around $l = 37°.5$, which goes down to $R = 10$ kpc.

From $l = 60°$ the density in the arm increases considerably, while the distance decreases from $R = 11$ kpc to 10 kpc at $l = 80°$. Between $l = 75°$ and $l = 82°.5$ it splits up and a fairly dense part goes out to $R = 10.8$ kpc again. From $l = 85°$ to the anti-centre the mean distance is 10.5 kpc. The mean height in the entire region is between $+100$ and $+200$ parsec, except for a deviation to -100 pc around $l = 77°.5$, $R = 9.7$ kpc.

At $l = 170°$ the arm may be traced again and is seen to move outward from 11 to 12.8 kpc. It lies at $z = 0$ pc here and tends to a negative height from $l = 210°$ onwards. At $l = 190°$ it is joined by a branch starting at about $l = 170°$, and running at $R = 12.4$ kpc, $z = -200$ pc.

c. Between the Perseus arm and the Orion arm two yet unnamed strong *intermediate arms* are seen. Around $l = 30°$ an arm branches off from the Orion arm at $R = 8.6$ kpc, to reach $R = 9.5$ kpc at $l = 47°.5$. At $l = 42°.5$, $R = 9$ to 10.5 kpc the situation is rather complex. The arm stops at $l = 70°$. It lies approximately at $z = 0$ pc over its whole length.

At $l = 175°$ an arm originates at $R = 9.7$ kpc, $z = 0$ pc, of which it is not clear whether it branches off from the Orion arm or from the Perseus arm. It is a fairly dense arm, and runs gradually outward to $R = 10.5$ kpc, $z = +150$ pc at $l = 220°$.

d. Two faint "*outer arms*" are visible with densities far below those of the main arms. One originates from the Perseus arm at $l = 12°.5$, $R = 12.5$ kpc, $z = +600$ pc and runs outward to about $R = 14$ kpc at $l = 35°$. It bends sharply inward again to rejoin the Perseus arm at $l = 45°$. Its mean height, between $+500$ and $+1000$ parsec, is very peculiar. The deviation becomes even larger by 100 parsec or so, if a correction to the standard plane is applied. A second faint arm begins to show at $l = 55°$, $R = 12$ kpc. It runs at a mean height of $+400$ pc up to $l = 65°$, from where the height gradually decreases to about 200 pc. No connection with the other faint arm could be found, although the heights suggest that both arms are part of the same outer arm. The arm can be traced as a separate arm to $l = 107°.5$, where the distance $R = 14$ kpc. A branch splits off at $l = 85°$ and moves

© Astronomical Institutes of The Netherlands • Provided by the NASA Astrophysics Data System

1957BAN....13..205W

TABLE 5

Mean values of z with respect to the Lund plane in 2 kpc intervals in r.

l	r	R	z	l	r	R	z	l	r	R	z	l	r	R	z
	kpc	kpc	pc		kpc	kpc	pc		kpc	kpc	pc		kpc	kpc	pc
215°	5	11.1	+ 200	105°	1	8.9	+ 15	75°	5	10.8	+ 225	47.°5	7	9.8	+ 20
	3	9.8	+ 50		3	10.6	+ 50		7	12.3	+ 350*		9	10.8	+ 125
	1	8.7	− 30		5	12.4	+ 185								
								72.5	1	8.5	+ 55	45	5	8.6	+ 25
210	5	11.4	− 10	102.5	1	8.9	+ 35		3	9.5	+ 20		7	9.6	+ 25
	3	10.0	− 50		3	10.5	+ 35		5	10.7	+ 170		9	10.8	+ 60
	1	8.8	0		5	12.2	+ 220		7	12.1	+ 315*				
												42.5	5	8.4	− 115
205	5	11.7	− 40	100	1	8.9	+ 10	70	1	8.5	+ 55		7	9.3	− 55
	3	10.1	+ 110		3	10.5	+ 45		3	9.4	− 10		9	10.5	+ 110
	1	8.9	− 65		5	12.1	+ 145		5	10.5	+ 160		11	11.9	+ 70*
									7	11.9	+ 350*				
200	3	10.3	+ 30	97.5	1	8.9	+ 20					40	1	8.0	+ 10
	1	8.8	− 10		3	10.4	+ 45	67.5	1	8.5	+ 45		3	7.9	− 40
					5	12.0	+ 170		3	9.2	0		5	8.2	+ 10
195	3	10.5	+ 45		7	13.8	+ 305*		5	10.3	+ 110		7	9.0	− 40
	1	8.9	+ 5						7	11.7	+ 355*		9	10.2	+ 70
				95	1	8.8	+ 30						11	11.6	+ 125*
190	3	10.6	+ 40		3	10.3	+ 50	65	1	8.5	+ 10		13	13.1	+ 425*
	1	9.0	+ 25		5	11.9	+ 165		3	9.1	0				
					7	13.6	+ 325*		5	10.2	+ 55	37.5	1	8.0	− 10
185	3	10.7	+ 70						7	11.5	+ 410*		3	7.8	− 40
	1	9.0	− 20	92.5	1	8.8	+ 20						5	8.9	0
					3	10.2	+ 100	62.5	1	8.4	+ 20		7	8.8	+ 55
180	3	10.8	0		5	11.8	+ 110		3	9.0	+ 10		9	9.9	+ 80
	1	9.1	− 10		7	13.5	+ 325*		5	10.0	+ 55		11	11.2	+ 165
									7	11.2	+ 270				
175	3	10.9	+ 65	90	1	8.8	− 60		9	12.7	+ 420*	35	1	7.9	− 25
	1	9.1	− 10		3	10.1	+ 95						3	7.6	− 40
					5	11.7	+ 245	60	1	8.4	+ 20		5	7.9	− 75
170	3	11.0	+ 15		7	13.3	+ 265*		3	8.9	+ 40		7	8.5	− 115
	1	9.1	− 10						5	9.8	+ 40		9	9.6	+ 40
				87.5	1	8.7	− 35		7	11.0	+ 250		11	10.9	+ 165
165	3	11.1	+ 10		3	10.0	+ 85		9	12.5	+ 350*		13	12.4	+ 495*
	1	9.2	0		5	11.6	+ 255								
					7	13.2	+ 275*	57.5	1	8.4	+ 20	32.5	1	7.9	− 25
160	3	11.2	+ 25						3	8.8	+ 10		3	7.6	− 45
	1	9.2	+ 15	85	1	8.7	+ 40		5	9.6	− 25		5	7.7	− 85
					3	10.0	+ 50		7	10.8	+ 165		7	8.2	− 125
135	1	9.2	+ 10		5	11.4	+ 305		9	12.2	+ 335*		9	9.2	+ 105
	3	11.2	+ 45		7	13.0	+ 275*						11	10.6	− 20
								55	1	8.3	+ 40		13	12.1	+ 350*
130	1	9.2	0	82.5	1	8.6	+ 50		3	8.7	+ 90				
	3	11.1	+ 80		3	9.9	+ 5		5	9.4	+ 55	30	1	7.8	− 35
					5	11.3	+ 315		7	10.6	+ 140		3	7.4	− 45
125	1	9.1	− 20		7	12.8	+ 320*		9	11.9	+ 360*		5	7.0	− 80
	3	11.0	+ 60										7	8.0	− 120
				80	1	8.6	+ 70	52.5	1	8.1	+ 50		9	9.0	− 95
120	1	9.1	+ 50		3	9.8	+ 10		3	8.6	+ 95		11	10.2	− 35
	3	10.9	+ 5		5	11.1	+ 270		5	9.2	− 30		13	11.7	− 120*
					7	12.6	+ 345*		7	10.3	+ 20				
115	1	9.1	+ 10						9	11.7	+ 225*	27.5	1	7.8	− 20
	3	10.8	+ 40										7	7.8	− 120
				77.5	1	8.5	+ 65	50	3	8.4	+ 110		9	8.6	− 170
110	1	9.0	+ 5		3	9.7	0		5	9.0	+ 80		11	9.9	− 50
	3	10.8	+ 70		5	11.0	+ 260		7	10.1	+ 20		13	11.4	+ 225*
					7	12.5	+ 335*		9	11.4	+ 220*		15	13.0	+ 510*
107.5	1	9.0	+ 15												
	3	10.7	+ 35	75	1	8.5	+ 60	47.5	3	8.2	+ 65	25	1	7.7	− 10
					3	9.5	+ 20		5	8.9	+ 50		3	7.1	− 55

* The numbers marked with an asterisk have not been used in the computations.

© Astronomical Institutes of The Netherlands • Provided by the NASA Astrophysics Data System

1957BAN....13..201W

TABLE 5 (*continued*)

l	r	R	z	l	r	R	z	l	r	R	z	l	r	R	z
	kpc	kpc	pc		kpc	kpc	pc		kpc	kpc	pc		kpc	kpc	pc
25°	7	7.5	− 115	12.°5	15	10.9	− 40*	0°	11	6.1	− 275	350°	19	11.9	− 220*
	9	8.3	− 180		17	12.6	− 460*		13	7.6	− 270				
	11	9.6	+ 55						15	9.2	− 240	347.5	1	7.3	+ 15
	13	11.0	+ 30	10	1	7.5	− 5		17	11.0	− 30*		3	5.5	− 65
	15	12.7	+ 280*		3	6.4	− 80						5	4.0	− 150
					5	5.7	− 155	357.5	1	7.4	+ 5		7	3.0	− 180
22.5	1	7.7	− 10		7	5.7	− 200		3	5.8	− 60		9	3.2	− 250
	5	6.8	− 75		9	6.4	− 235		5	4.6	− 135		11	4.4	− 345
	7	7.2	− 125		11	7.6	− 220		9	4.6	− 250		13	6.1	− 295
	9	8.1	− 160		13	8.9	− 180		11	5.8	− 290		15	7.9	− 355
	11	9.2	− 35		15	10.5	− 85		13	7.3	− 265		17	9.7	− 410
	13	10.7	+ 60		17	12.3	− 145*		15	8.9	− 325		19	11.6	− 185*
									17	10.7	− 40*		21	13.6	− 165*
20	1	7.6	− 10	7.5	1	7.5	− 5								
	3	6.8	− 55		3	6.2	− 75	355	1	7.3	+ 5	345	1	7.2	+ 15
	7	6.9	− 140		5	5.5	− 140		3	5.7	− 55		3	5.4	− 55
	9	7.8	− 125		9	6.0	− 245		5	4.5	− 140		5	3.8	− 155
	11	8.8	− 55		11	7.2	− 230		9	4.3	− 255		7	2.7	− 190
	13	10.3	− 10		13	8.5	− 295		11	5.4	− 310		9	2.9	− 260
	15	11.9	+ 200*		15	10.2	− 130		13	7.0	− 265		11	4.2	− 350
					17	12.0	+ 265*		15	8.6	− 400		13	5.8	− 320
17.5	1	7.6	− 10						17	10.4	− 370		15	7.6	− 385
	3	6.7	− 60	5	1	7.4	0		19	12.3	− 100*		17	9.5	− 465
	7	6.6	− 140		3	6.1	− 65						19	11.4	− 390*
	9	7.4	− 170		5	5.3	− 120	352.5	1	7.3	+ 10				
	11	8.5	− 50		9	5.7	− 245		3	5.7	− 60	342.5	1	7.2	+ 5
	13	10.0	− 60		11	6.8	− 250		5	4.4	− 140		3	5.3	− 55
	15	11.6	+ 95*		13	8.2	− 280		7	3.6	− 185		13	5.6	− 315
					15	9.9	− 390		9	3.9	− 245		15	7.4	− 370
15	1	7.6	− 10						11	5.1	− 335		17	9.3	− 345
	3	6.6	− 65	2.5	1	7.4	− 5		13	6.6	− 270		19	11.3	− 255
	7	6.3	− 175		3	6.0	− 70		15	8.3	− 355				
	9	7.1	− 195		5	5.1	− 120		17	10.2	− 245	340	1	7.2	0
	11	8.1	− 160		9	5.4	− 245						3	5.3	− 65
	13	9.6	− 30		11	6.5	− 255	350	1	7.3	+ 15		13	5.4	− 320
	15	11.2	+ 25*		13	8.0	− 255		3	5.6	− 65		15	7.3	− 440
					15	9.5	− 105		5	4.1	− 145		17	9.2	− 305
12.5	1	7.6	− 50		17	11.3	+ 20*		7	3.3	− 170		19	11.2	− 295
	3	6.5	− 80						9	3.6	− 250				
	7	6.0	− 175	0	1	7.4	− 5		11	4.8	− 345	335	8.2	1.1	− 190
	9	6.7	− 215		3	5.9	− 65		13	6.4	− 275	330	8.2	0.4	− 210
	11	7.9	− 220		5	4.9	− 115		15	8.1	− 225				
	13	9.2	− 155		9	5.0	− 255		17	10.0	− 445	325	8.2	0.4	− 190

* The numbers marked with an asterisk have not been used in the computations.

outward to more than 15 kpc at $l = 105°$. Beyond this longitude the densities become too small to give reliable density contours, but hydrogen can be traced farther than 20 kpc from the centre at $l = 130°$. It is very striking that at the other side of the anti-centre, up to $l = 180°$, no hydrogen is detected beyond $R = 14$ kpc.

16. *Determination of a mean galactic plane.*

An inspection of the fairly constant tilt in the arms in the outer parts of the Galactic System, and of the very smooth increase of the negative $\bar{z}$ with r in the inner parts of the system (Figure 7 of the following article) leaves the impression of a well-determined plane in which the neutral hydrogen is distributed. In order to arrive at a reliable determination of such a plane observations of the southern hemisphere are needed. We have tried, however, with the present data, to obtain some idea about the accuracy with which a plane may be determined and about the remaining deviations from the mean plane.

Because of the incompleteness in the southern data results presented below should not be considered as a new determination of the galactic pole. The International Astronomical Union has formed a subcommission (33b) to assemble all the available optical and radio data and make recommendations about a new pole to be generally adopted within the next few years.

© Astronomical Institutes of The Netherlands • Provided by the NASA Astrophysics Data System

1957BAN..13..217W

The data used in the preliminary determination are given in Table 5. For the region $R < 8.2$ kpc they are taken from Figure 7 of the following article, which is based on the values of $\bar{z}$ in Table 9 of that article [1]). The points for $l = 335°$, 330° and 325° are the mean values of the z co-ordinate in the long wings of the profiles in the central directions, which are attributed to hydrogen in a highly turbulent region within $R = 3$ kpc [2]).

For the region $R > 8.2$ kpc the fundamental data are the positions in latitude b_{max} of points of maximum intensity. These are taken from the plots of intensity against latitude for each longitude in 40 kc/s intervals, described in section 11b. From these data the curves of Figure 7 of SCHMIDT's paper were extended beyond $R = 8.2$ kpc, omitting the process of smoothing in circles between two values of R, as has been done for $R < 8.2$ kpc; the extensions showed many more irregularities. The mean values of $\bar{z}$ in 2-kpc intervals in r, determined graphically from the curves, are given in Table 5.

The points obtained in the region $R < 8.2$ kpc are much more reliable for two reasons: *a*. The force K_z, which together with the random motions determines the concentration toward the galactic plane, is much stronger in the central regions. According to SCHMIDT [3]), the ratio between K_z, at $z = 0.2$ kpc, for $R = 4.1$ kpc and $R = 9.2$ kpc is 11. The observations show that the hydrogen distribution in the central parts is much smoother than in the outer parts. Possibly, a better equilibrium is reached in these regions. Also, deviations from a smooth model of mass distribution tend to cancel in the much more massive central parts. *b*. The points in the region $R < 8.2$ kpc are determined from direct latitude scans, and not from a combination of a number of independent line profiles spaced by 2°.5.

The numbers marked with an asterisk in Table 5 have not been used in the computations. They refer to the regions with very small density and often very large deviations from the plane, with $R > 11 - 12$ kpc. The points for which data are given in Table 5 are much closer together in the neighbourhood of the sun than at large distances. The number of points per unit area in the galactic plane is, in fact, inversely proportional to the distance from the sun r. If all points are given equal weight, the region near the sun strongly influences the solution. There are two ways to reach the equivalent of an even distribution of points over the whole plane. *a*) Mean points can be determined in areas of, for example, 4 kpc^2. *b*) The points can be weighted in proportion to their distance to the sun r. Alternative *b*) has been used in the computations. The equation of condition for a point r, z, l is

$$z = x + y\,r\cos l + u\,r\sin l, \qquad (21)$$

where $-x$ is the z co-ordinate of the sun with respect to the new plane, $y = \operatorname{tg}\Delta\cos L$ and $u = \operatorname{tg}\Delta\sin L$. The angle between the standard plane and the new plane is Δ, while the north pole of the new plane has $l = L$ and $b = B = 90° - \Delta$. A least-squares solution, using all points, gave $x = -26$ pc, $L = 299°$, $\Delta = 1°.86$. If only the points with $R < 8.2$ kpc (Figure 7 of the following article) are used, the solution is $x = -23$ pc $\pm$ 10, $L = 332° \pm 8$, $\Delta = 1°.37 \pm .07$, m.e. (solution A). The large difference between the two solutions is due to a systematic curvature. While in the inner parts of the Galactic System all the hydrogen is below the standard plane, it tends to bend upwards in the adjacent regions of the outer parts. This is particularly noticeable in the region $10° < l < 40°$. The data available at present suggest a dish-like shape for the galactic system. Apparently the hydrogen density in the outer parts is so small that cloud collisions or exchange of matter with the inner parts cannot make up for the disturbing effects of large scale motion. We thought it better, therefore, to give much more weight to the inner parts, where the plane seems well determined. The residuals from the solution for the part $R < 8.2$ kpc (solution A) for all points were plotted as a function of R. The mean values of these residuals $\bar{\Delta}$ are given in Table 6.

TABLE 6

Mean z co-ordinates $\bar{\Delta}$ with respect to a plane through the hydrogen layer for $R < 8.2$ kpc (solution A), and weights w assigned to the points in solution B.

R	$\bar{\Delta}$	w
kpc	pc	
<7.9	0	20
8.2	24	11.2
8.6	32	5.0
9.0	48	2.2
9.3	64	1.2
10.0	96	0.5
10.3	125	0.3
10.6	180	0.2
10.9	230	0
11.2	300	0

The points were weighted according to the formula $w = \frac{5}{\bar{\Delta}^2} \cdot \frac{\mu^2}{\bar{r}}$ where $\mu = \pm 96$ pc is the mean error of unit weight and $\bar{r} = 9.1$ is the mean weight for

[1]) M. SCHMIDT, *B.A.N.* **13**, 247 (No. 475, fourth paper), 1957.
[2]) K. K. KWEE, C. A. MULLER and G. WESTERHOUT, *B.A.N.* **12**, 211 (No. 458), 1954.
[3]) *B.A.N.* **13**, 15 (No. 468), 1956.

© Astronomical Institutes of The Netherlands • Provided by the NASA Astrophysics Data System

1957BAN....13..201W

TABLE 7

Two solutions for a new galactic plane.
A: based on the region $R < 8.2$ kpc only.
B: weighted points for $R > 8.2$ kpc included.

	Height		Galactic pole			
	$-x$	m.e.	L	m.e.	B	m.e.
	pc	pc				
A	+23	±10	332°	±8°	88°.63	±.07
B	+26	± 7	322	±4	88.56	±.05

the part $R < 8.2$ kpc. The final solution, B, was made using all the points (with the exception of those marked with an asterisk) with weights $w \times r$. The two solutions are given in Table 7.

Comparison of the two solutions shows that, even though the points with $R > 8.2$ kpc have very small weights, they still shift the pole considerably. It will be very interesting to see whether the deviations found in the outer parts are also present, or compensated, in the regions invisible from Kootwijk.

The deviations z of the points of maximum hydrogen density from the plane determined in solution B are given as contours in Figure 7.

They are drawn in the picture of the Galactic System shown on Plate A. The parts with -25 pc $< z <$ $+25$ pc are shaded. The figure illustrates the small deviations from the mean plane in the central parts of the Galactic System, and the large values of z in the outer parts. No definite correlation of the contours with individual spiral arms is noticeable.

Galactic pole determinations have been made previously by many authors. VAN TULDER [1]) in 1942 compiled all available data and determined a mean pole at $L = 330°.7$, $B = 88°.9$ and a distance from the sun to the plane of $+13.5$ pc.

17. *Mean hydrogen densities.*

For comparison with other stellar systems, it is desirable to have a picture of the distribution of hydrogen in the galactic plane as a function of the distance from the centre R. Mean values of n_H between circles at intervals of 1 kpc in R, determined from plate B for the region discussed in this and the following paper, are given in Table 8 and Figure 6.

The Orion and Sagittarius arms are visible, even in this smoothed picture, as one maximum, while the Perseus arm, which is almost circular, gives a second maximum. The maximum near $R = 4.5$ kpc is very uncertain, as it is due to a very small part of one of the inner arms, the density of which is not well determined.

TABLE 8

Mean hydrogen densities between circles around the galactic centre.

R	$\bar{n}_H$	R	$\bar{n}_H$
kpc	at/cm³	kpc	at/cm³
3-4	0.33	9-10	0.41
4-5	.72	10-11	.55
5-6	.68	11-12	.40
6-7	.97	12-13	.21
7-8	.72	13-14	.09
8-9	.48	14-15	.04

In *B.A.N.* No. 458 [2]) the mean hydrogen density in the region $R < 2$ kpc was determined from the low-intensity wings of the line profiles in the central regions. Its value, $n_H = 0.4$ cm^{-3}, is given as a dotted line in the figure.

No definite correlation of n_H with galactocentric longitude has been found. In the region $R > 8$ kpc, between $l = 20°$ and $l = 340°$, the densities are systematically lower than in other directions, while the opposite effect holds for the region $R < 8$ kpc.

FIGURE 6

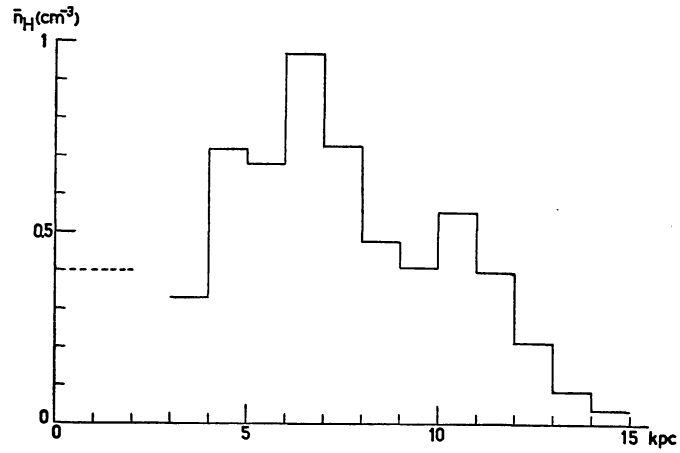

Mean hydrogen densities as a function of R.
Dotted line: *B.A.N.* No. 458.

Many thanks are due to Prof. J. H. OORT for his constant encouragement, to Prof. H. C. VAN DE HULST for his help and advice, and to numerous persons who assisted in various parts of the reductions, in particular Messrs KIEL and CASPARIE.

[1]) *B.A.N.* **9**, 315 (No. 353), 1942.

[2]) K. K. KWEE, C. A. MULLER and G. WESTERHOUT, *B.A.N.* **12**, 211 (No. 458), 1954.

© Astronomical Institutes of The Netherlands • Provided by the NASA Astrophysics Data System

1957BAN....13..201W

PLATE B

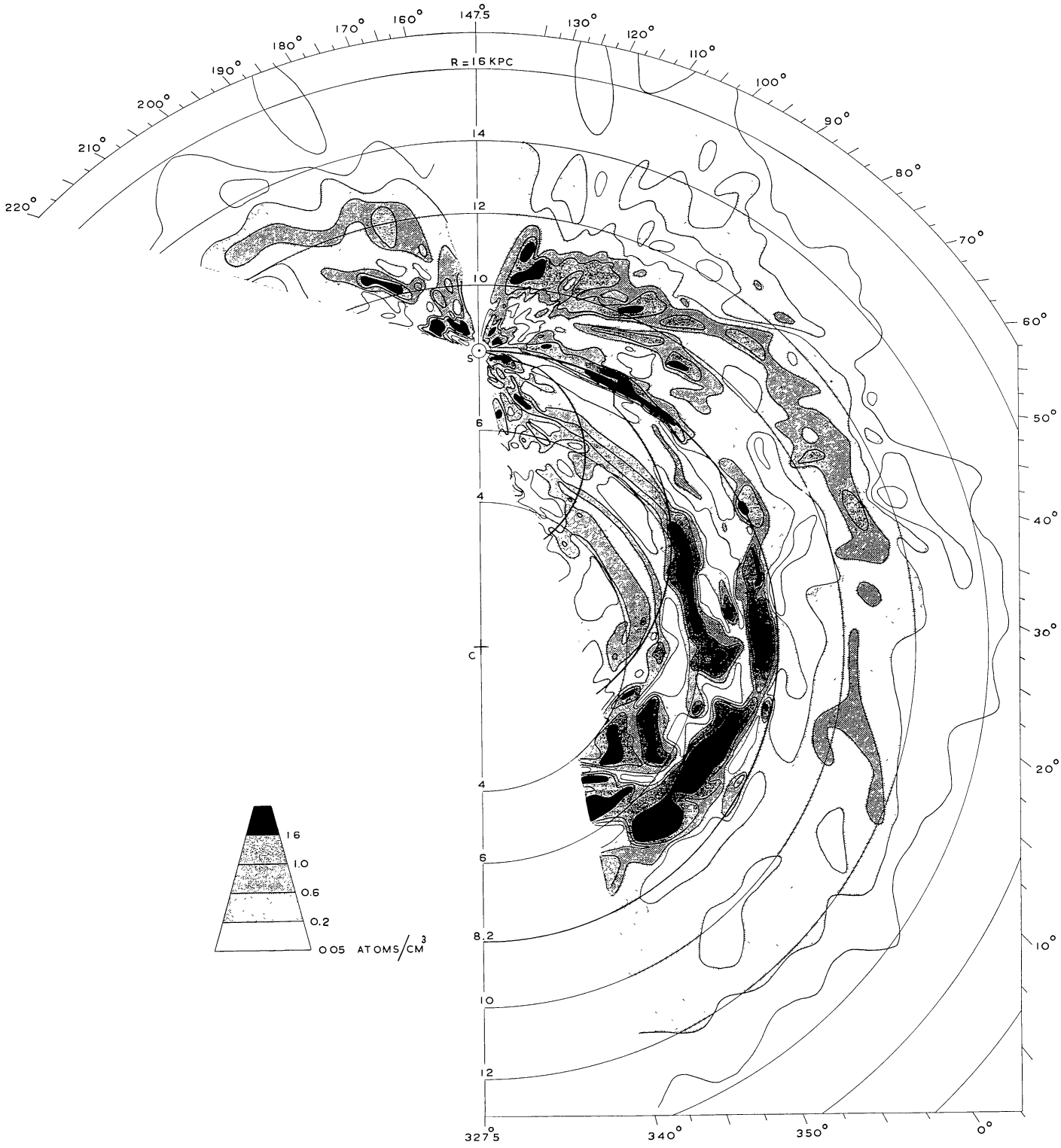

Contours of equal density of neutral hydrogen in the Galactic System. The maximum densities in the z-direction are projected on the galactic plane, and contours are drawn through the points.

© Astronomical Institutes of The Netherlands • Provided by the NASA Astrophysics Data System

1958BAN....13..219B

FIGURE 7

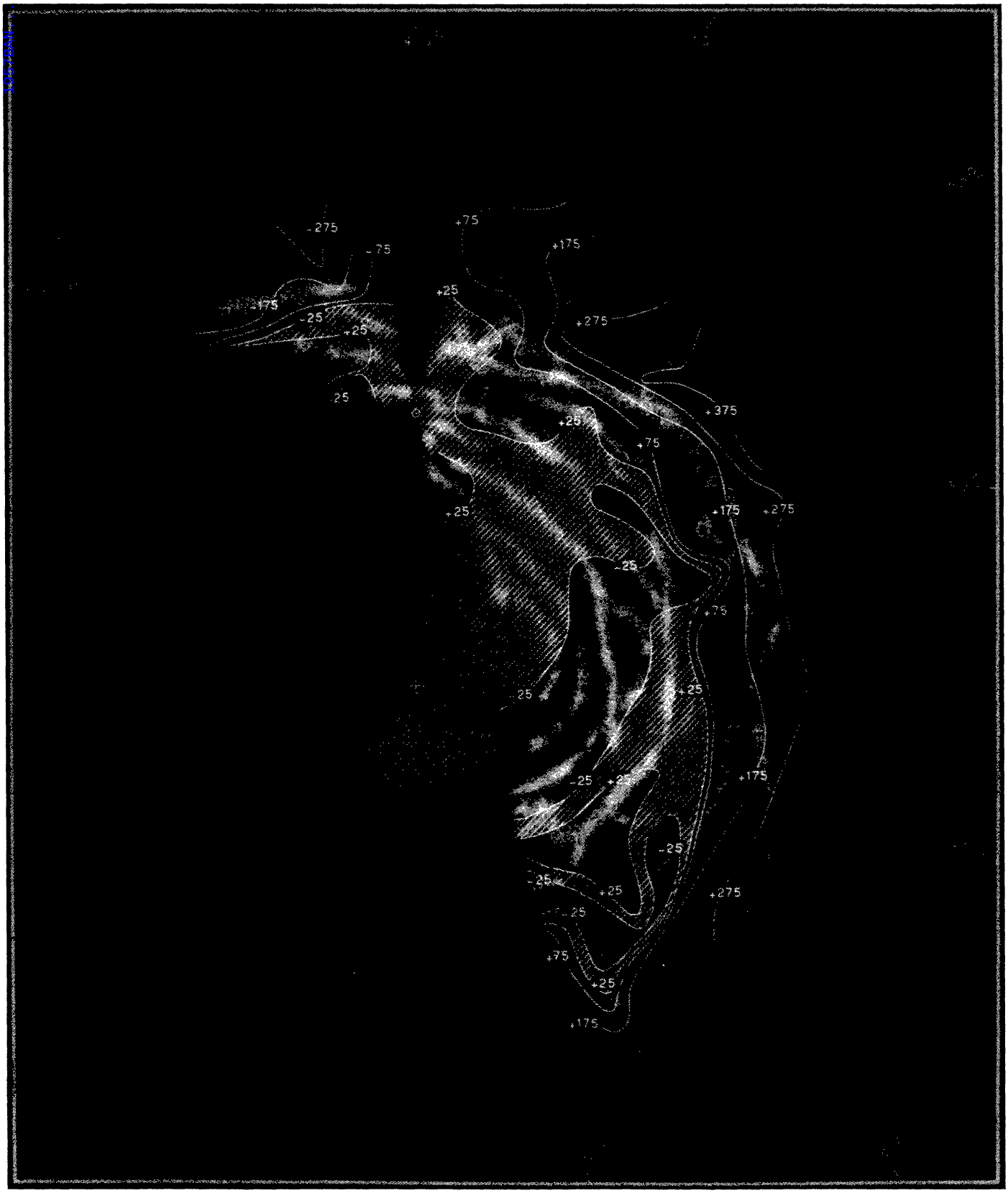

Contours of equal height z above a mean galactic plane (solution B). The parts with -25 pc $< z < +25$ pc are shaded.

© Astronomical Institutes of The Netherlands • Provided by the NASA Astrophysics Data System

1957BAN....13..201

FIGURE 8a

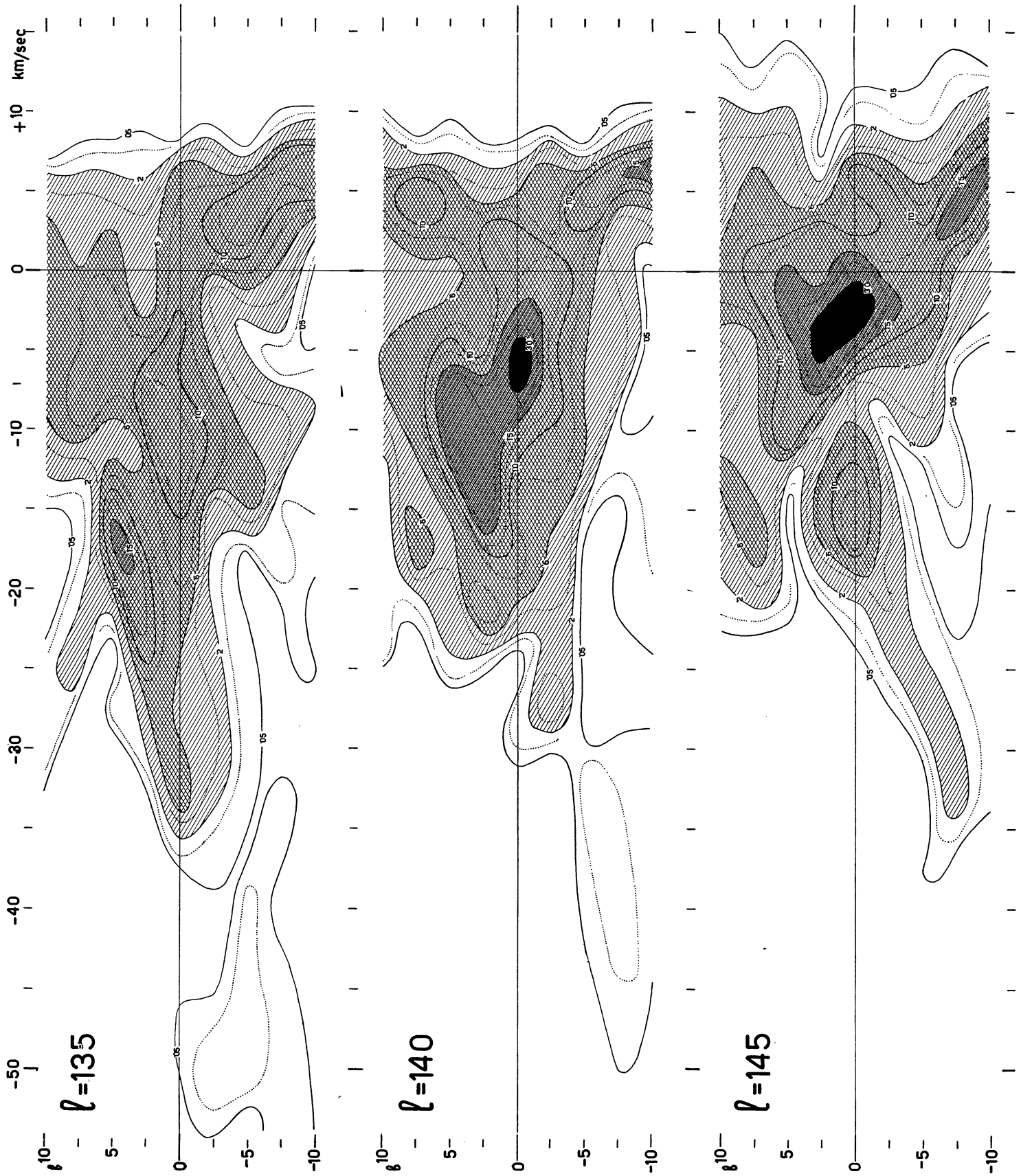

© Astronomical Institutes of The Netherlands • Provided by the NASA Astrophysics Data System

1957BAN....13..

FIGURE 8b

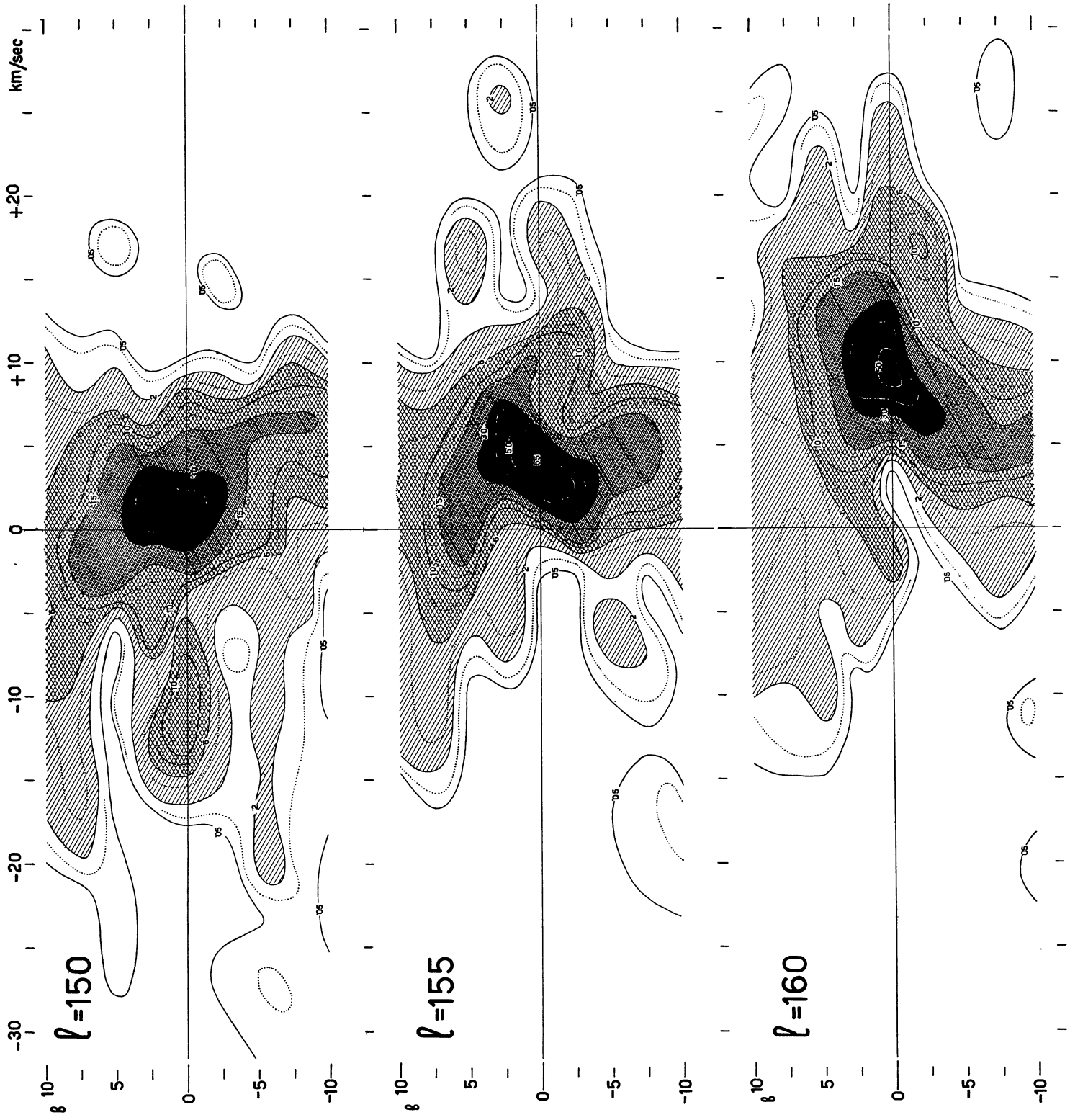

Contours of optical depth, corrected for cloud velocities, in planes perpendicular to the galactic plane, as a function of radial velocity and latitude. The contours for $\tau' = .1, .4, .8, 1.2$ and 2.0 are dotted.

© Astronomical Institutes of The Netherlands • Provided by the NASA Astrophysics Data System

1957BAN....13..201W

FIGURE 9

Contours of hydrogen density in planes perpendicular to the galactic plane, in co-ordinate system l, r, z.
r = distance from the sun. R = distance from the galactic centre.

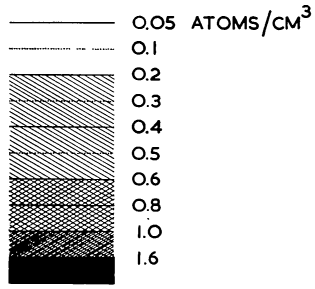

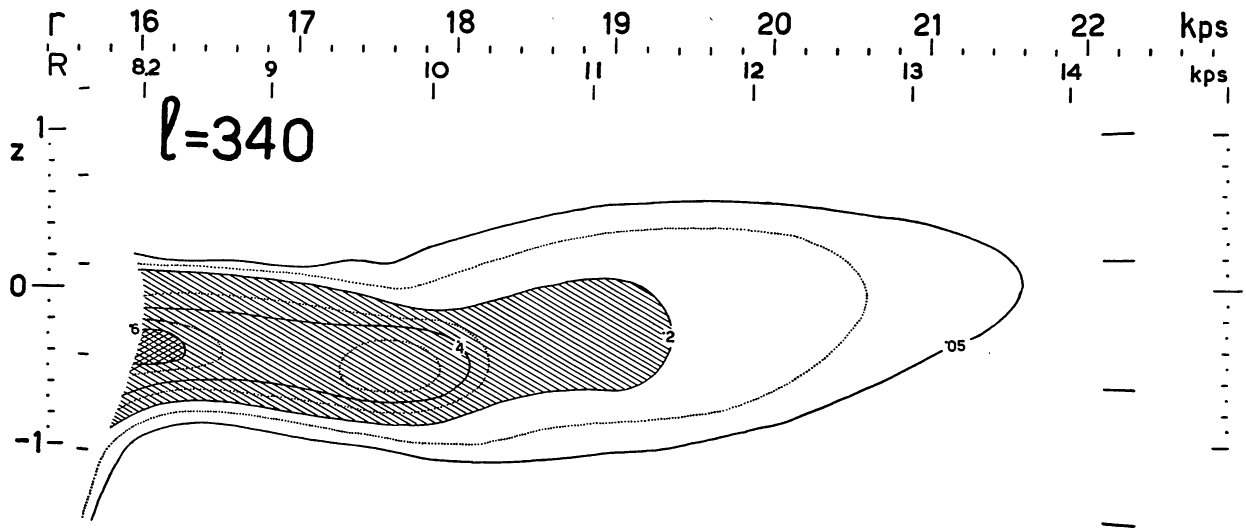

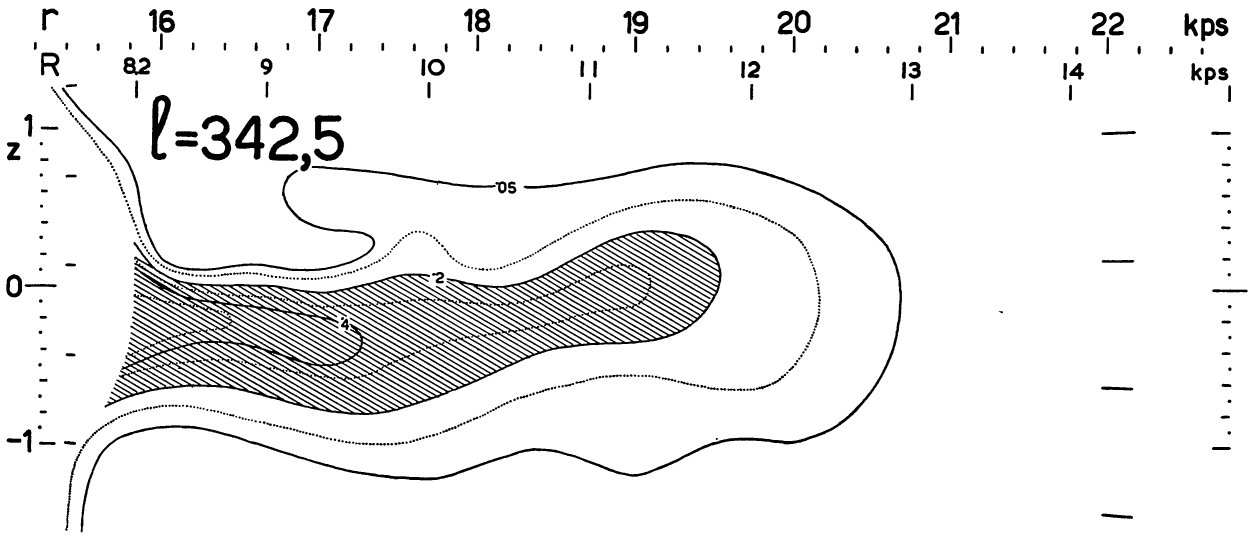

© Astronomical Institutes of The Netherlands • Provided by the NASA Astrophysics Data System

1957BAN....13..201W

FIGURE 9 (*continued*)

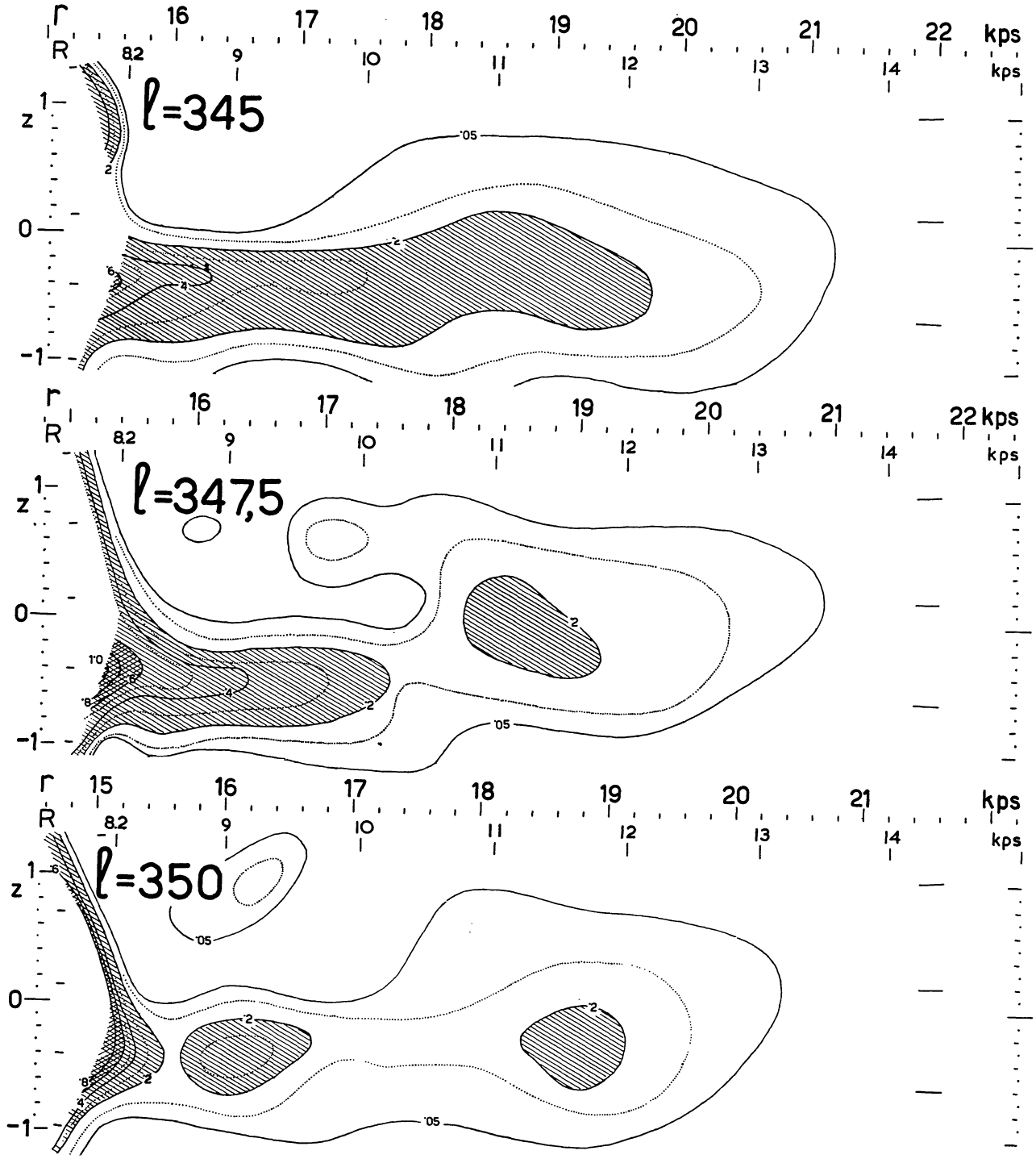

© Astronomical Institutes of The Netherlands • Provided by the NASA Astrophysics Data System

1957BAN....13..201W

FIGURE 9 (*continued*)

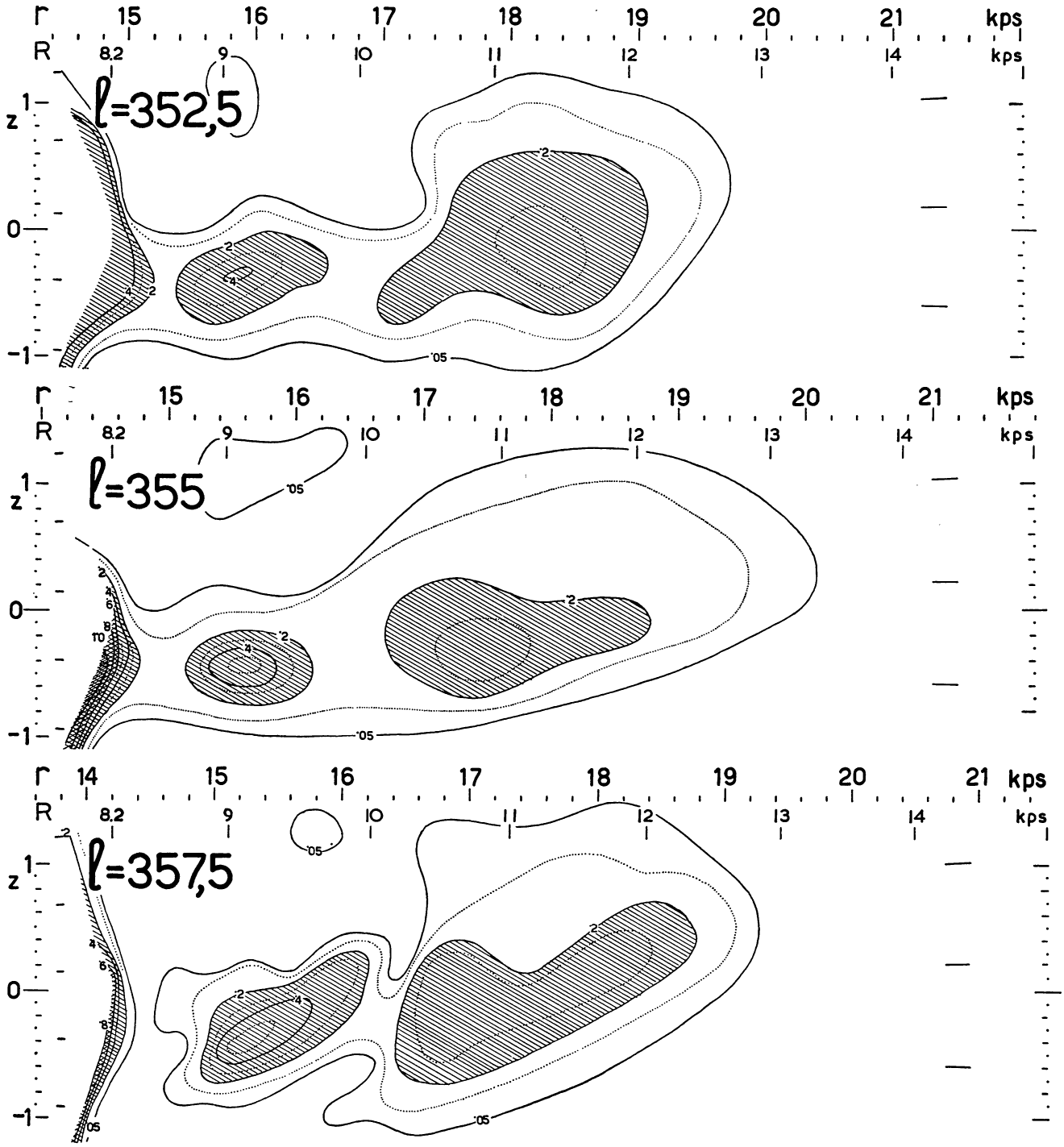

© Astronomical Institutes of The Netherlands • Provided by the NASA Astrophysics Data System

1957BAN....13..201W

FIGURE 9 (*continued*)

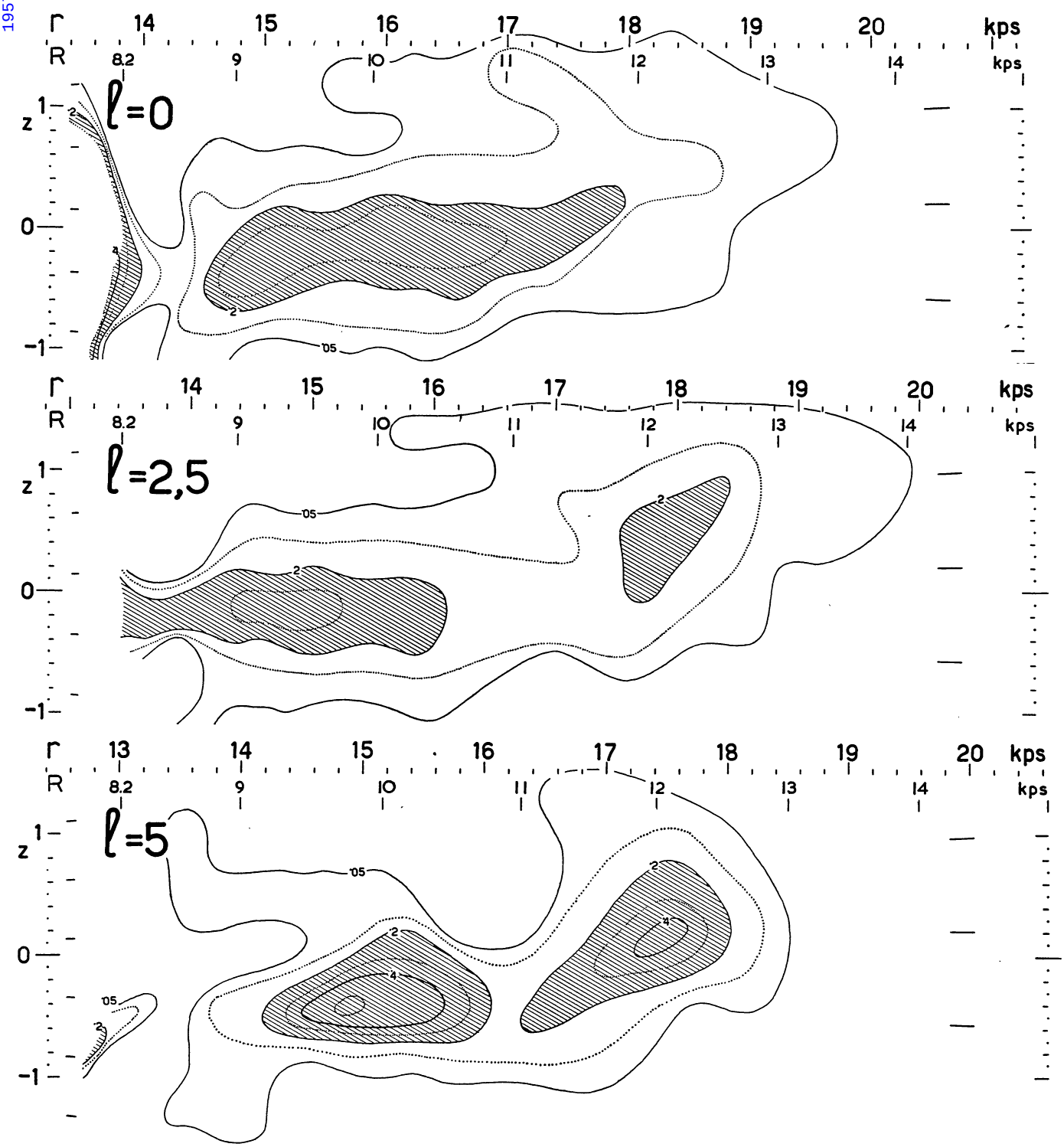

© Astronomical Institutes of The Netherlands • Provided by the NASA Astrophysics Data System

1957BAN....13..201W

FIGURE 9 (*continued*)

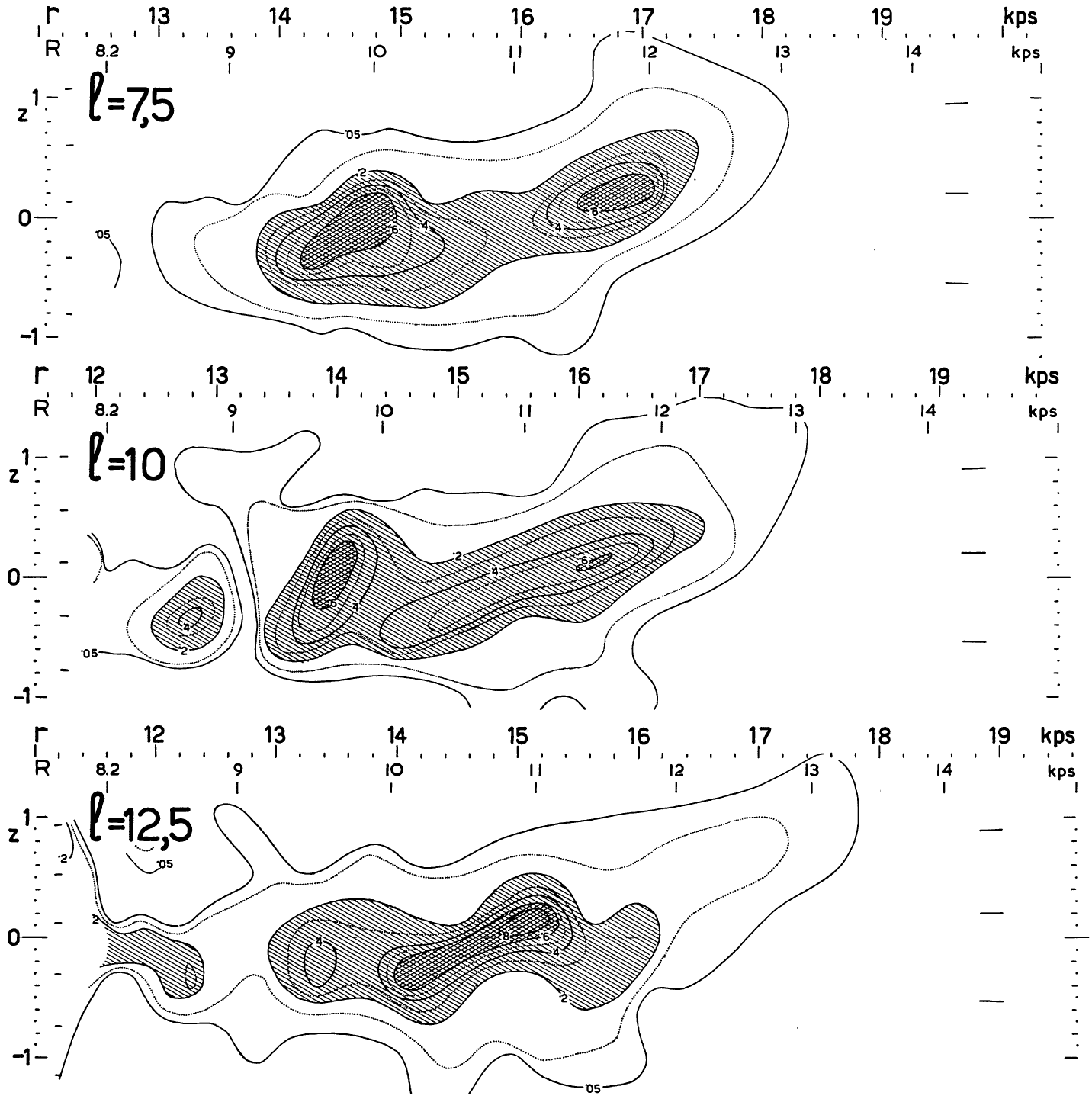

© Astronomical Institutes of The Netherlands • Provided by the NASA Astrophysics Data System

1957BAN....13..201W

FIGURE 9 (*continued*)

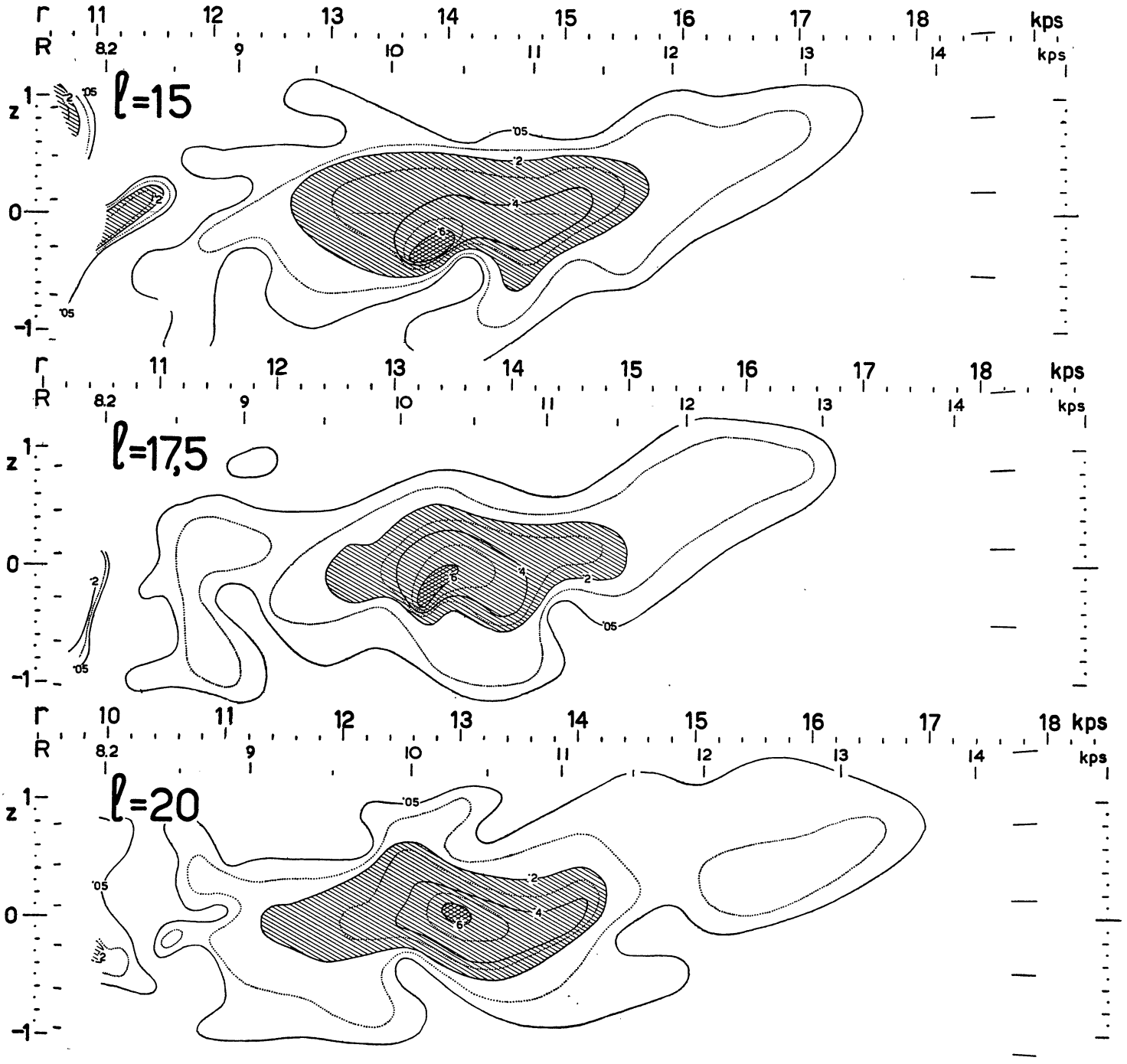

© Astronomical Institutes of The Netherlands • Provided by the NASA Astrophysics Data System

1957BAN....13..229

FIGURE 9 (*continued*)

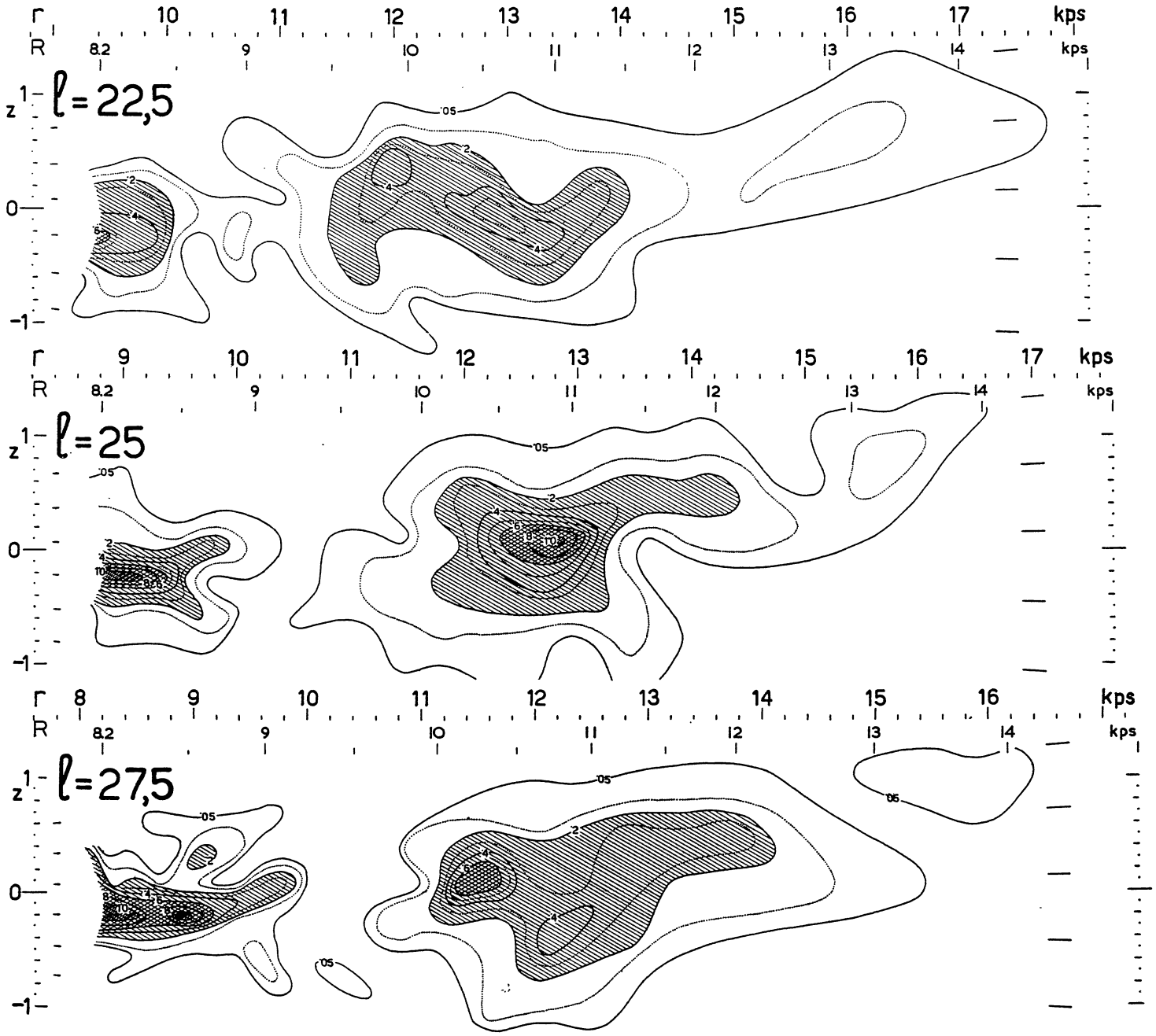

© Astronomical Institutes of The Netherlands • Provided by the NASA Astrophysics Data System

1957BAN....13..201W

FIGURE 9 (*continued*)

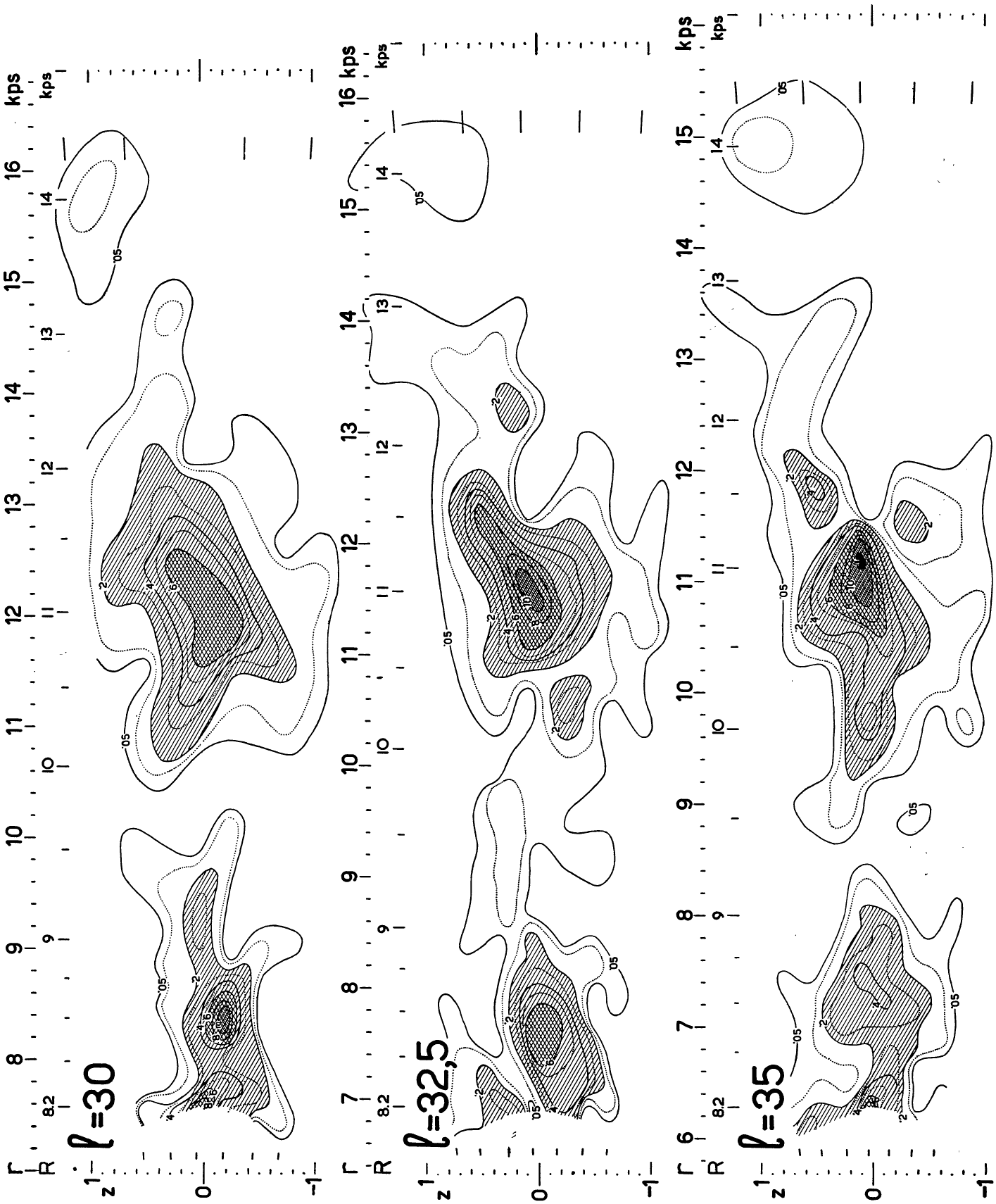

© Astronomical Institutes of The Netherlands • Provided by the NASA Astrophysics Data System

1973AN....13..201W

FIGURE 9 (*continued*)

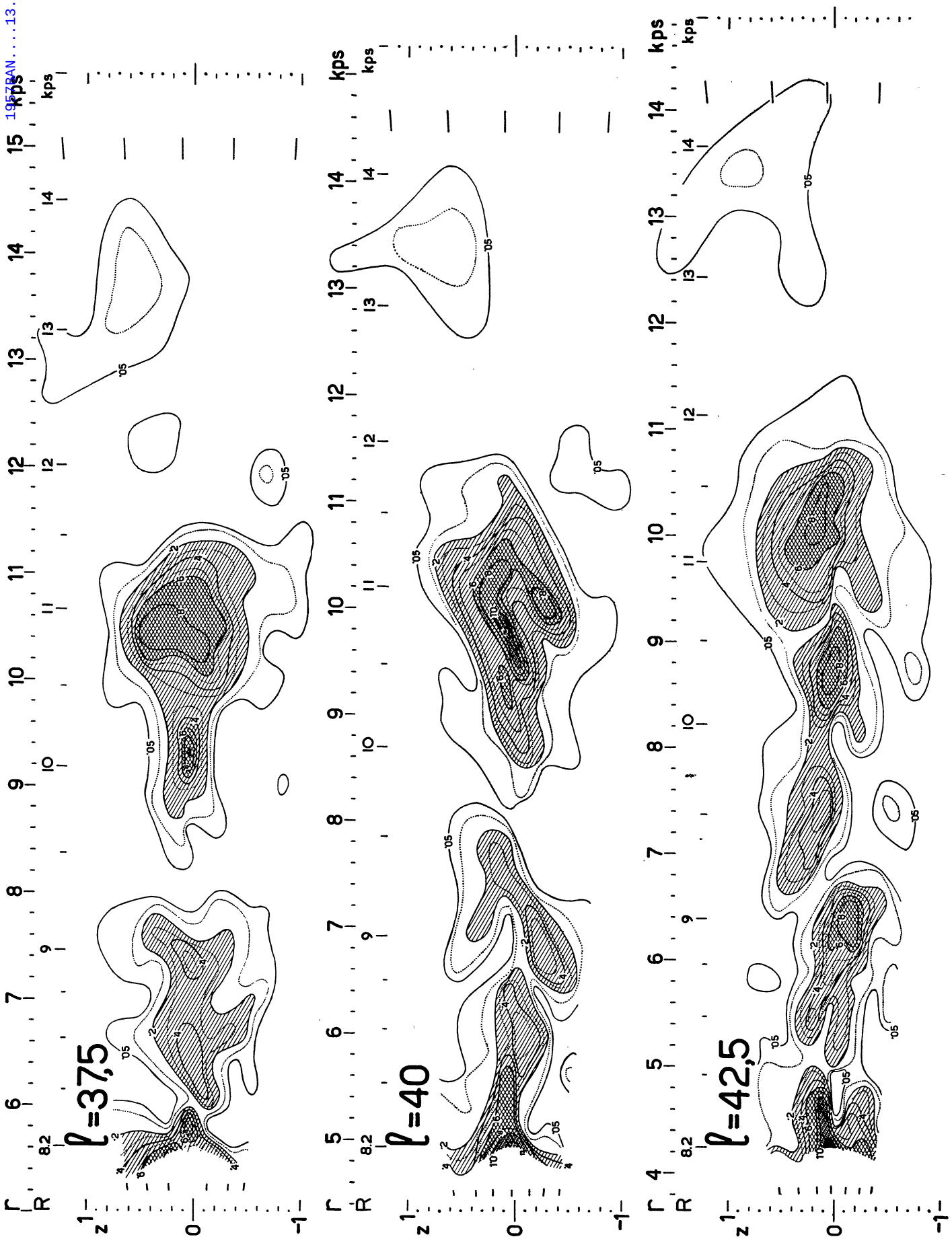

© Astronomical Institutes of The Netherlands • Provided by the NASA Astrophysics Data System

1957BAN....13..201W

FIGURE 9 (*continued*)

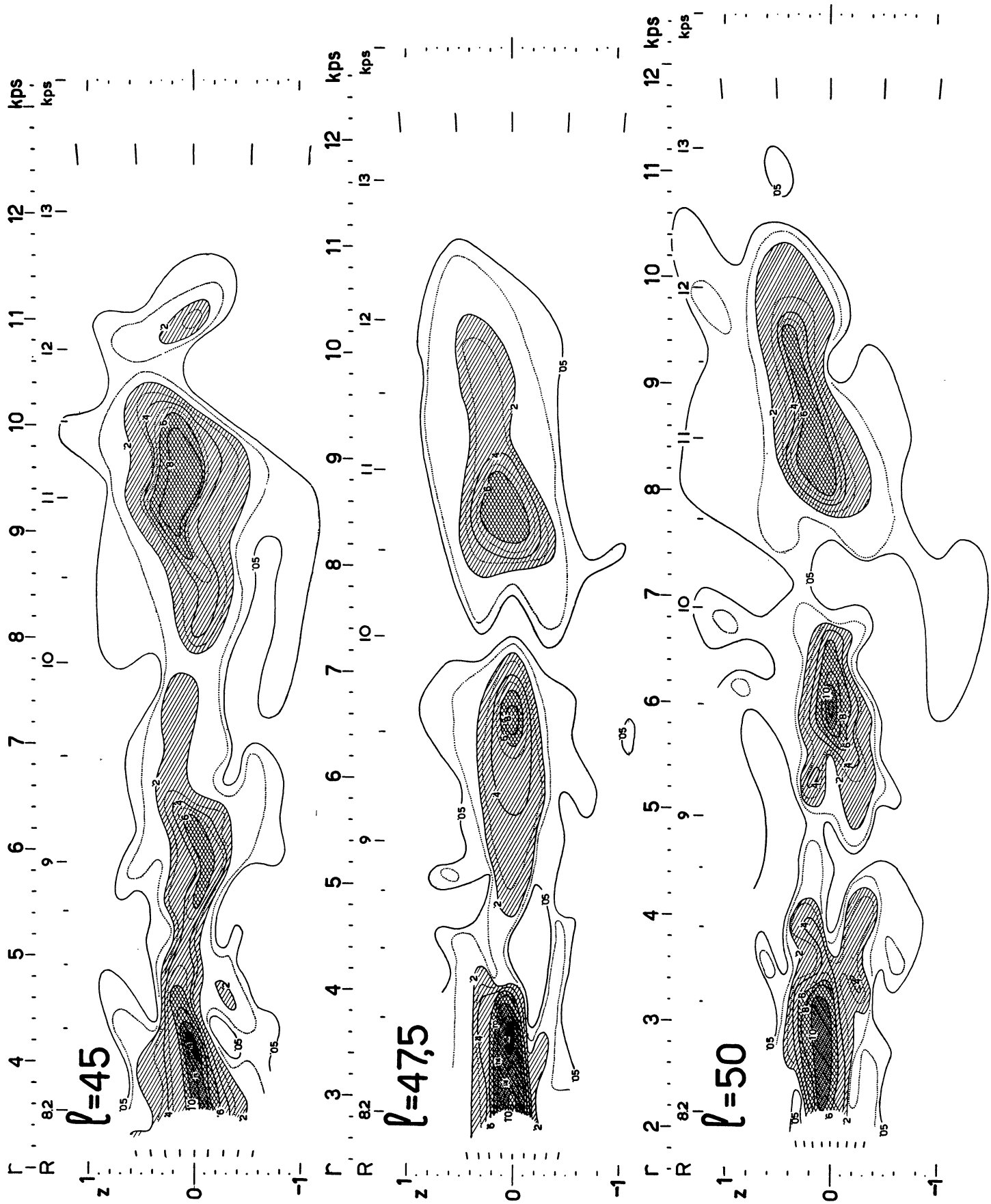

© Astronomical Institutes of The Netherlands • Provided by the NASA Astrophysics Data System

1957BAN....13..201W

FIGURE 9 (*continued*)

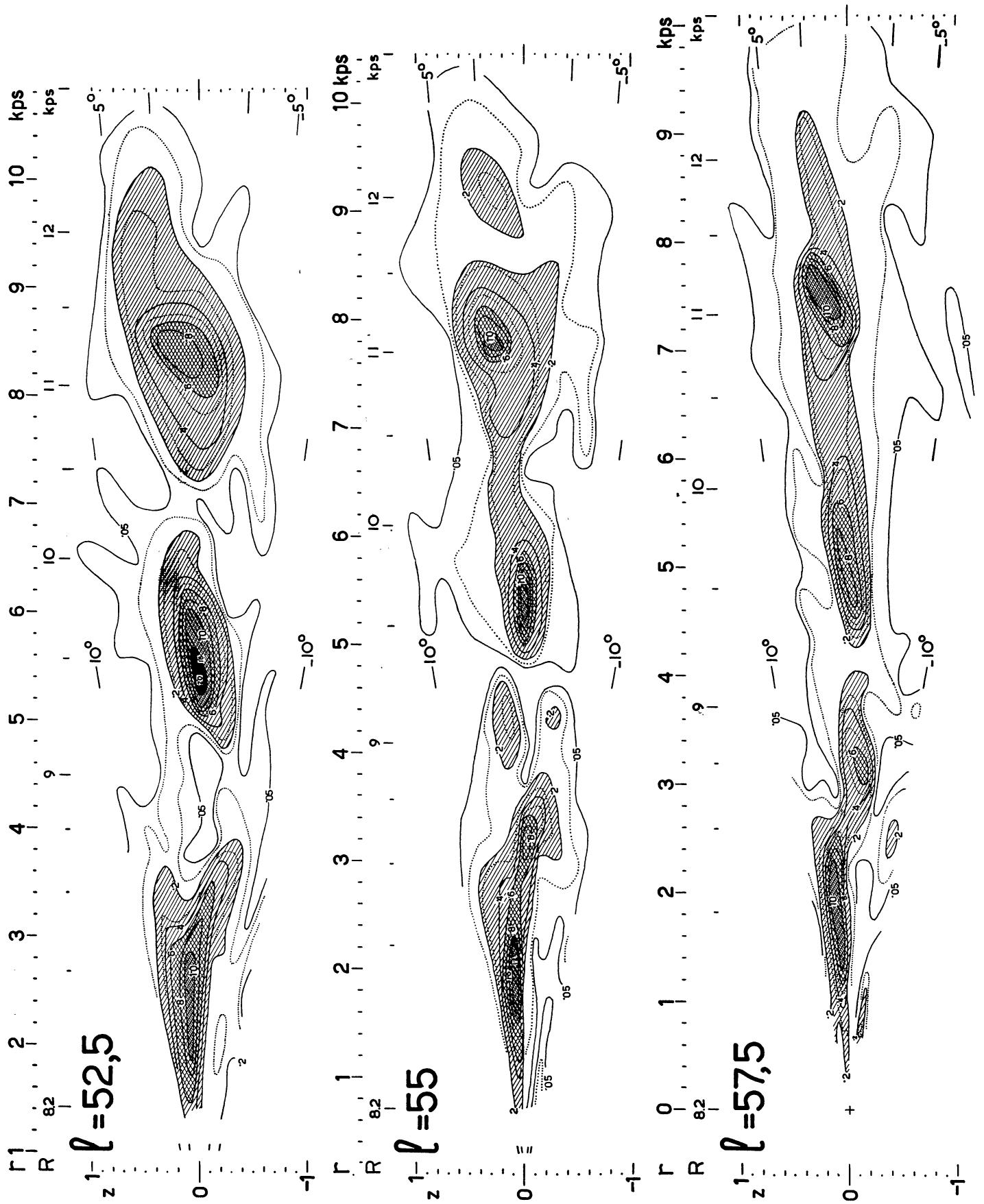

© Astronomical Institutes of The Netherlands • Provided by the NASA Astrophysics Data System

1957BAN....13..201W

FIGURE 9 (*continued*)

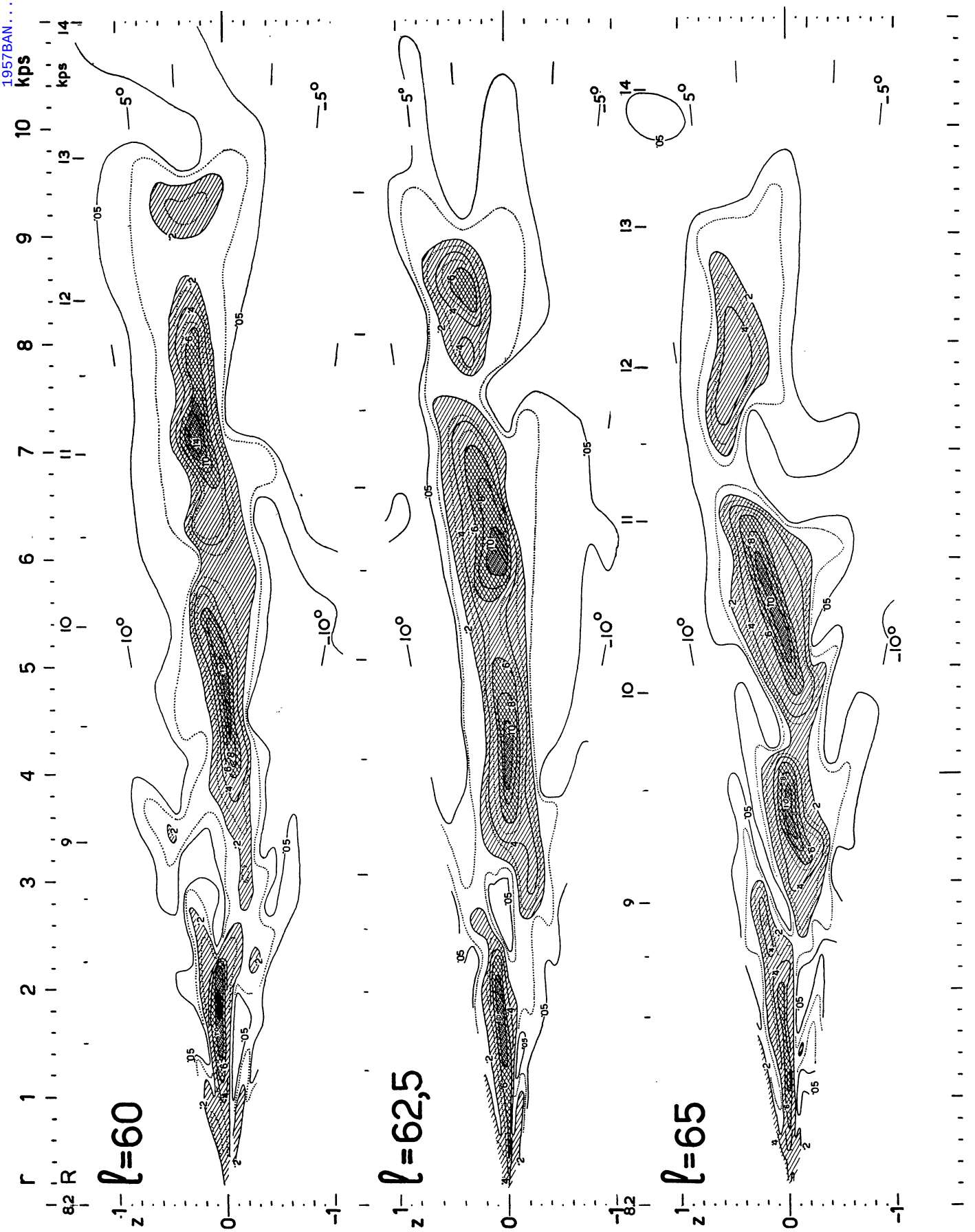

© Astronomical Institutes of The Netherlands • Provided by the NASA Astrophysics Data System

1957BAN....13..201W

FIGURE 9 (*continued*)

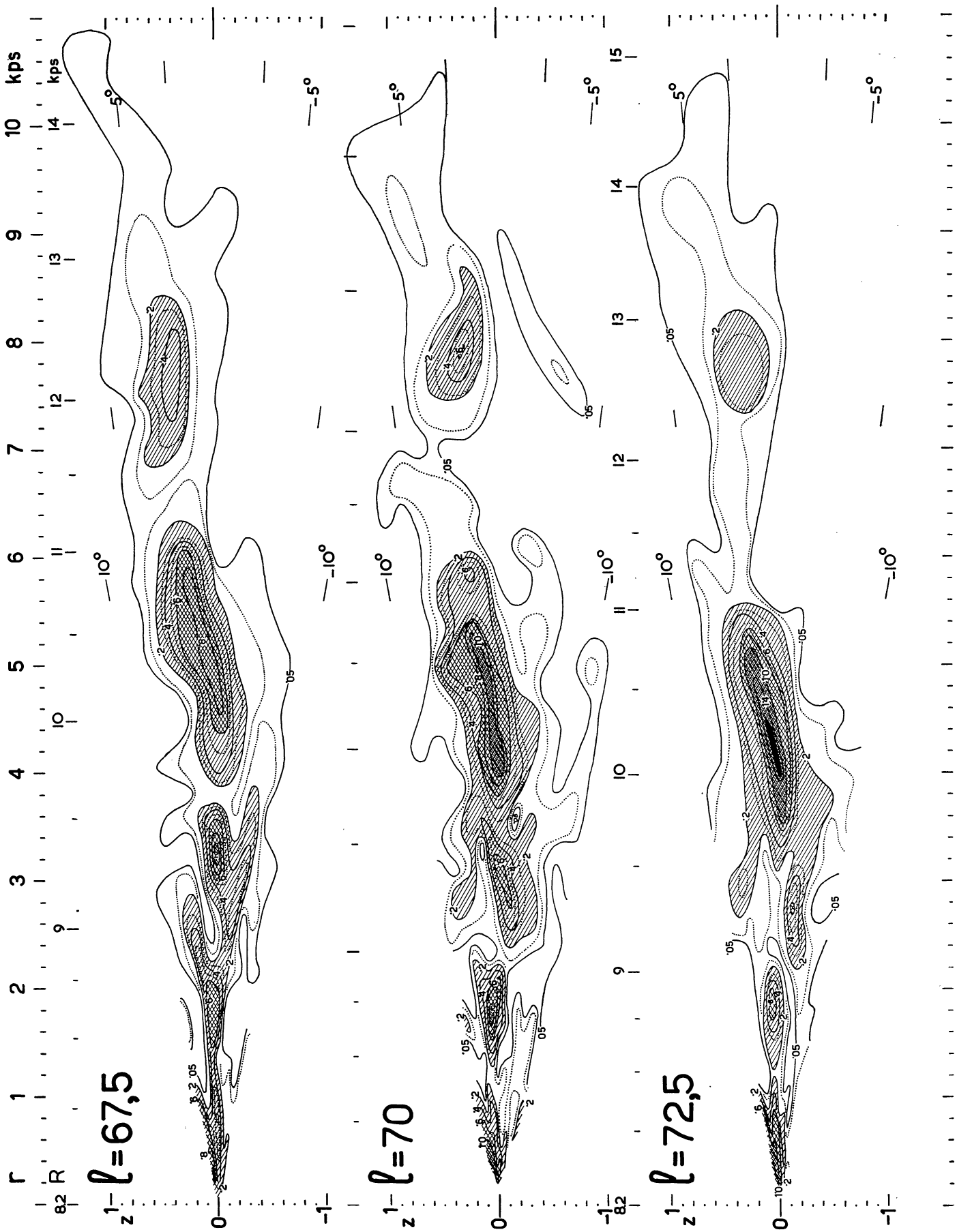

© Astronomical Institutes of The Netherlands • Provided by the NASA Astrophysics Data System

1957BAN....13..201W

FIGURE 9 (*continued*)

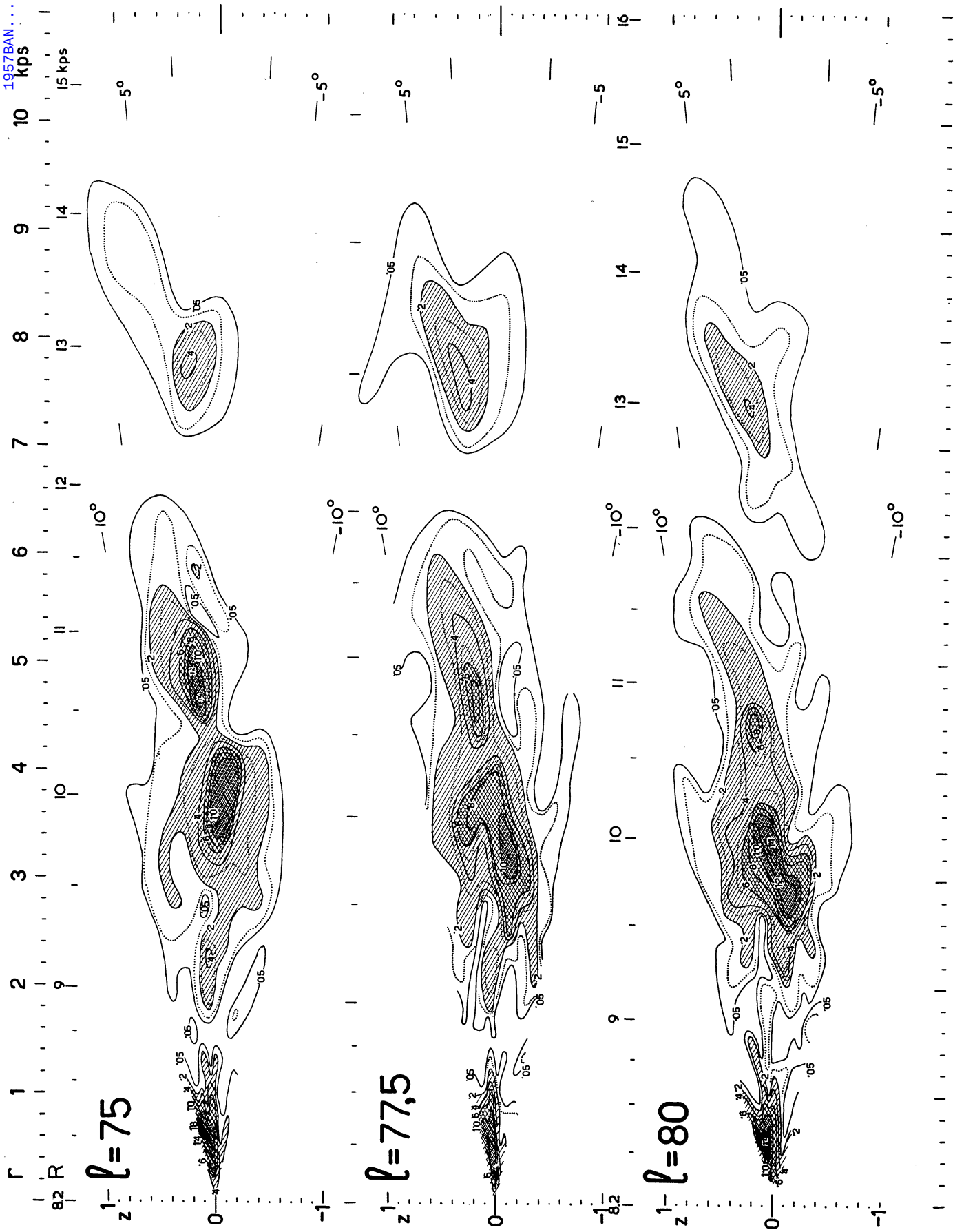

© Astronomical Institutes of The Netherlands • Provided by the NASA Astrophysics Data System

1957BAN....13..201W

FIGURE 9 (*continued*)

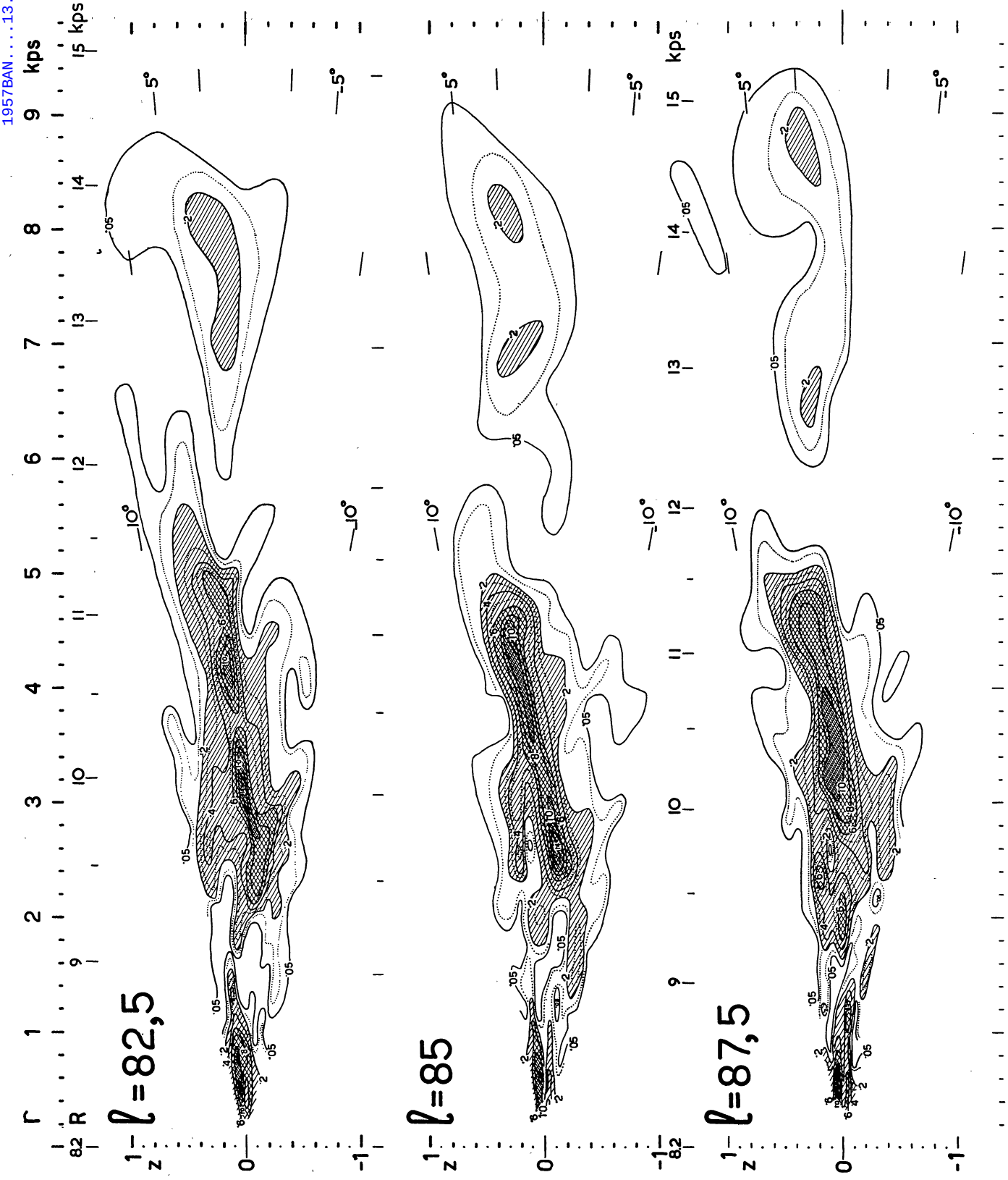

© Astronomical Institutes of The Netherlands • Provided by the NASA Astrophysics Data System

1957BAN....13..201W

FIGURE 9 (*continued*)

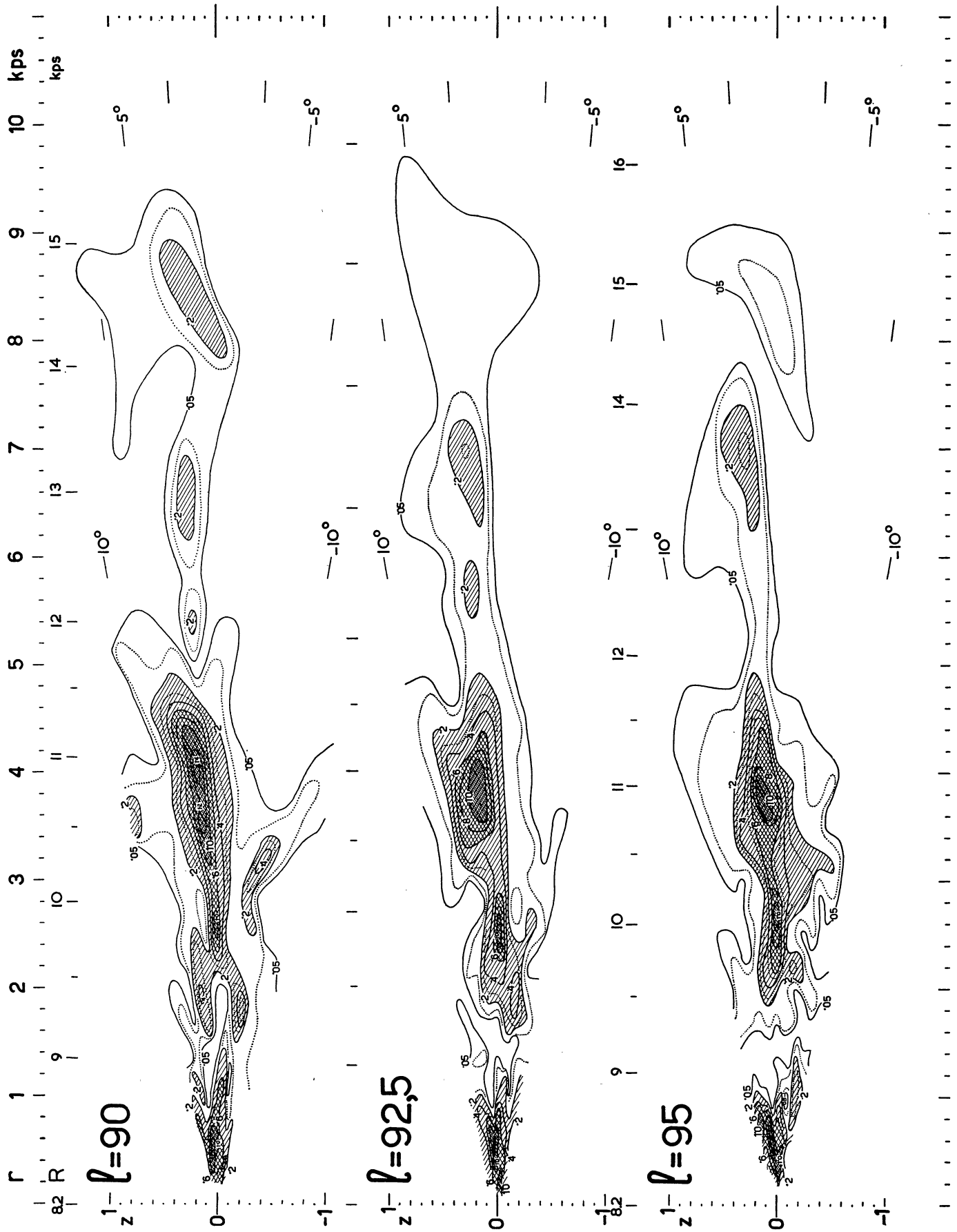

© Astronomical Institutes of The Netherlands • Provided by the NASA Astrophysics Data System

1957BAN....13..201W

FIGURE 9 (*continued*)

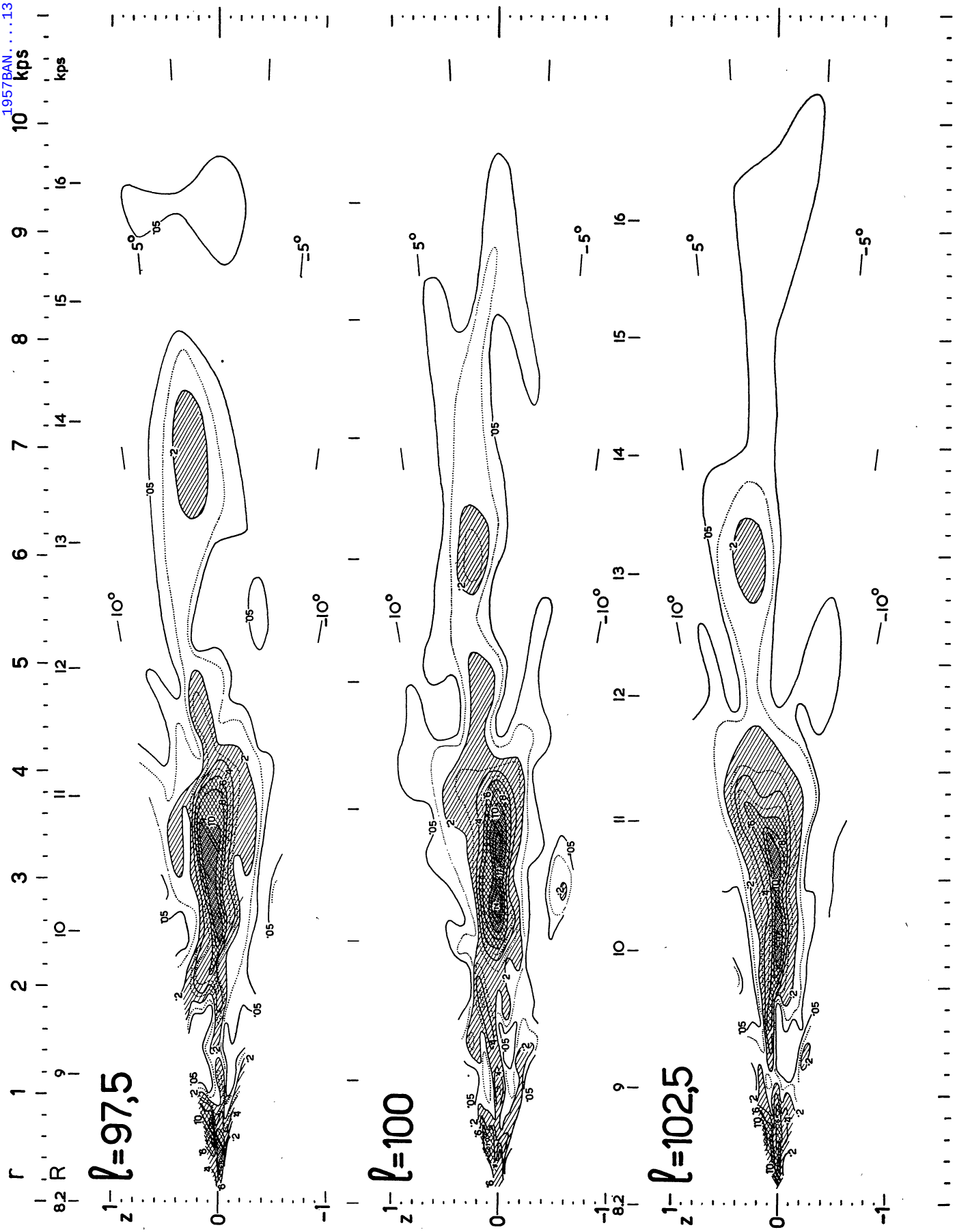

© Astronomical Institutes of The Netherlands • Provided by the NASA Astrophysics Data System

1957BAN....13..201W

FIGURE 9 (*continued*)

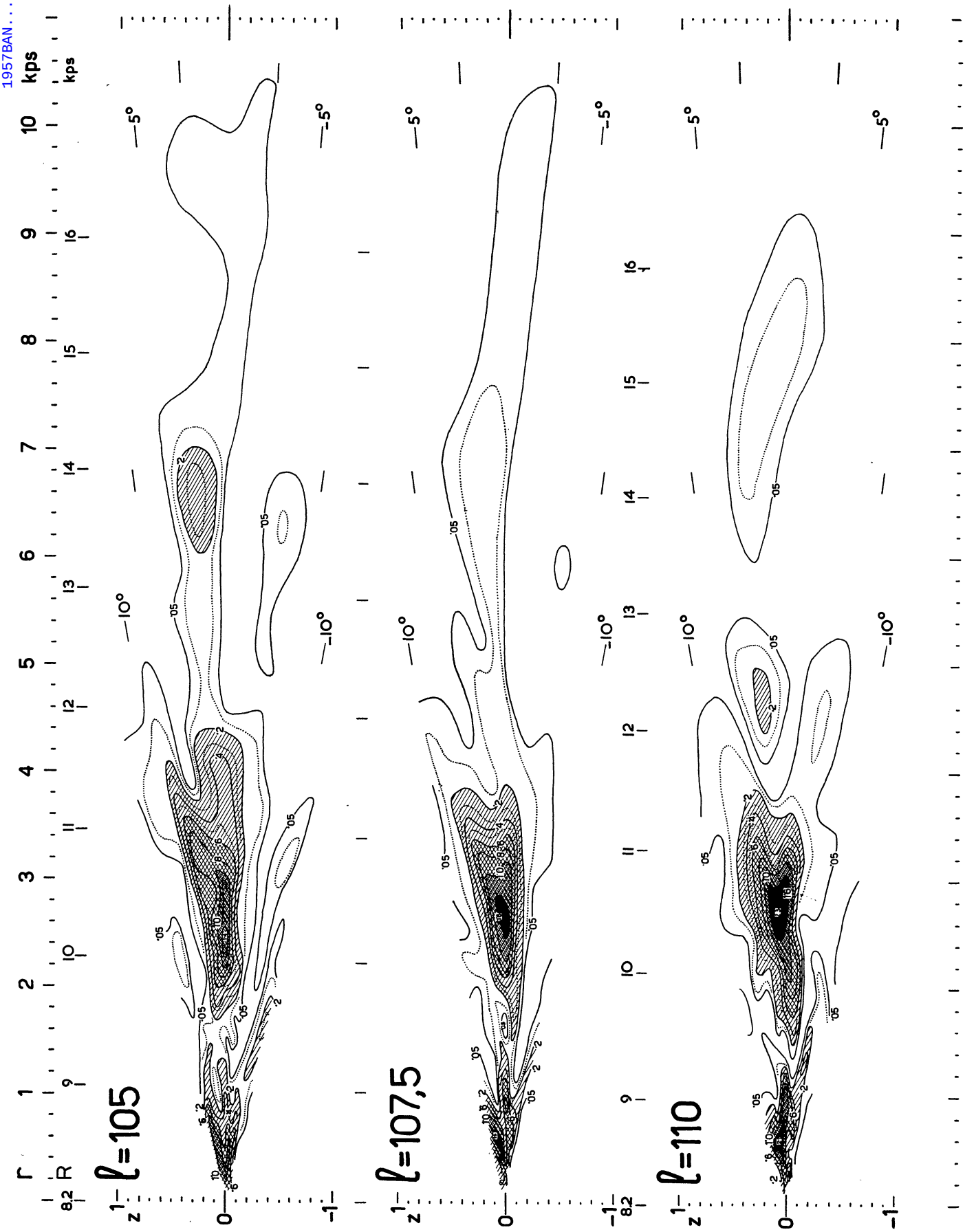

© Astronomical Institutes of The Netherlands • Provided by the NASA Astrophysics Data System

1957BAN....13..201W

FIGURE 9 (*continued*)

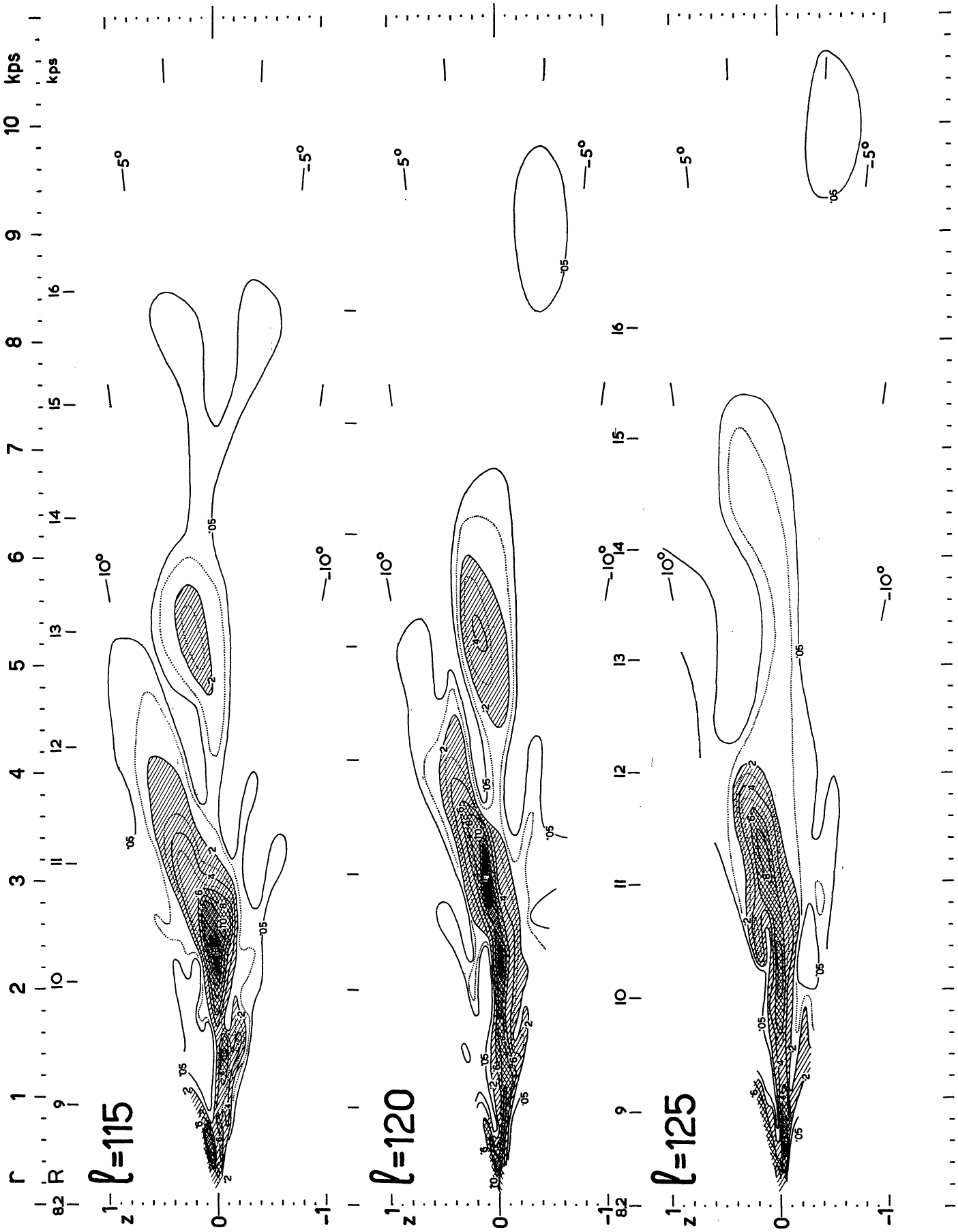

© Astronomical Institutes of The Netherlands • Provided by the NASA Astrophysics Data System

1957BAN....13..201W

FIGURE 9 (*continued*)

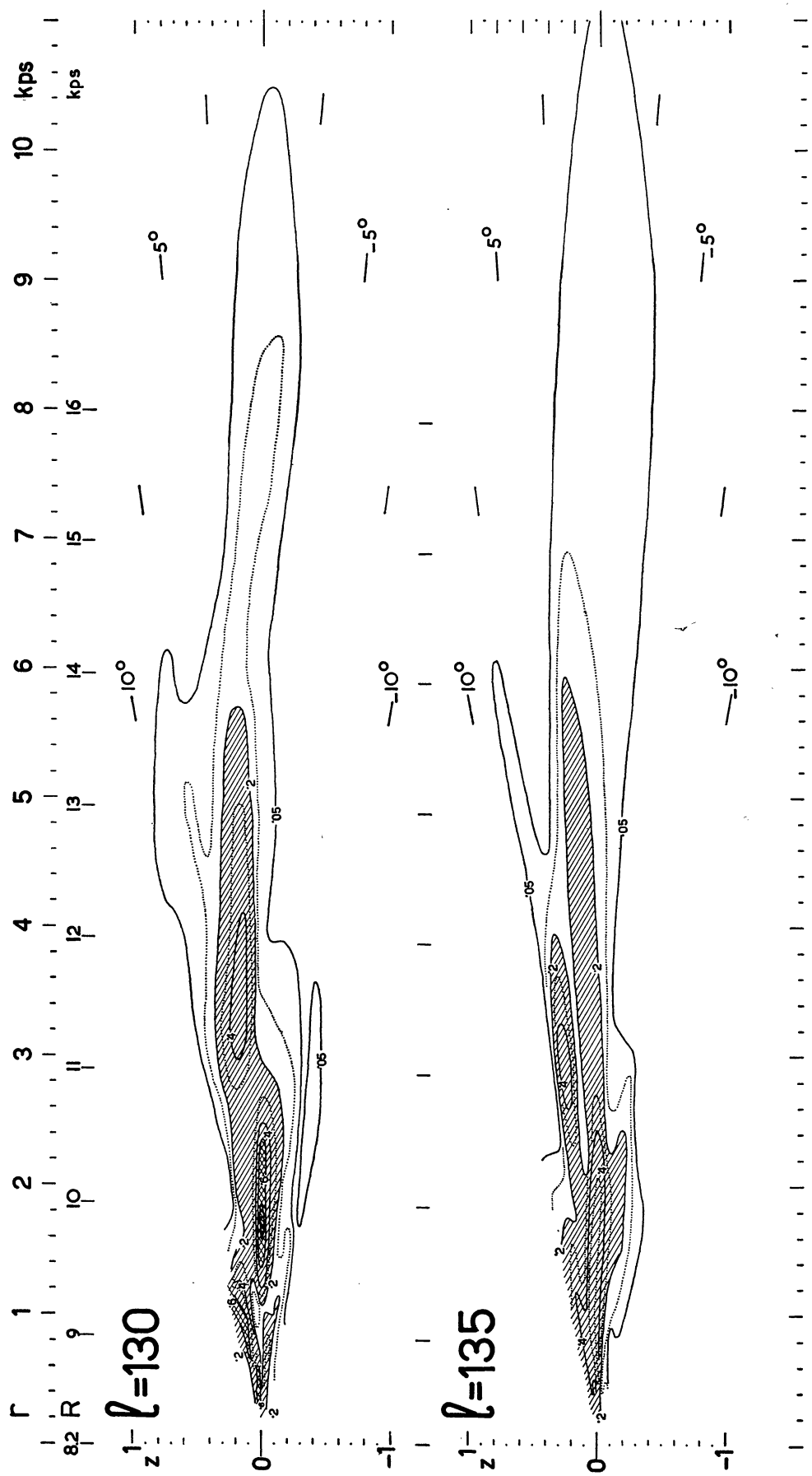

© Astronomical Institutes of The Netherlands • Provided by the NASA Astrophysics Data System

1957BAN....13..201W

FIGURE 9 (*continued*)

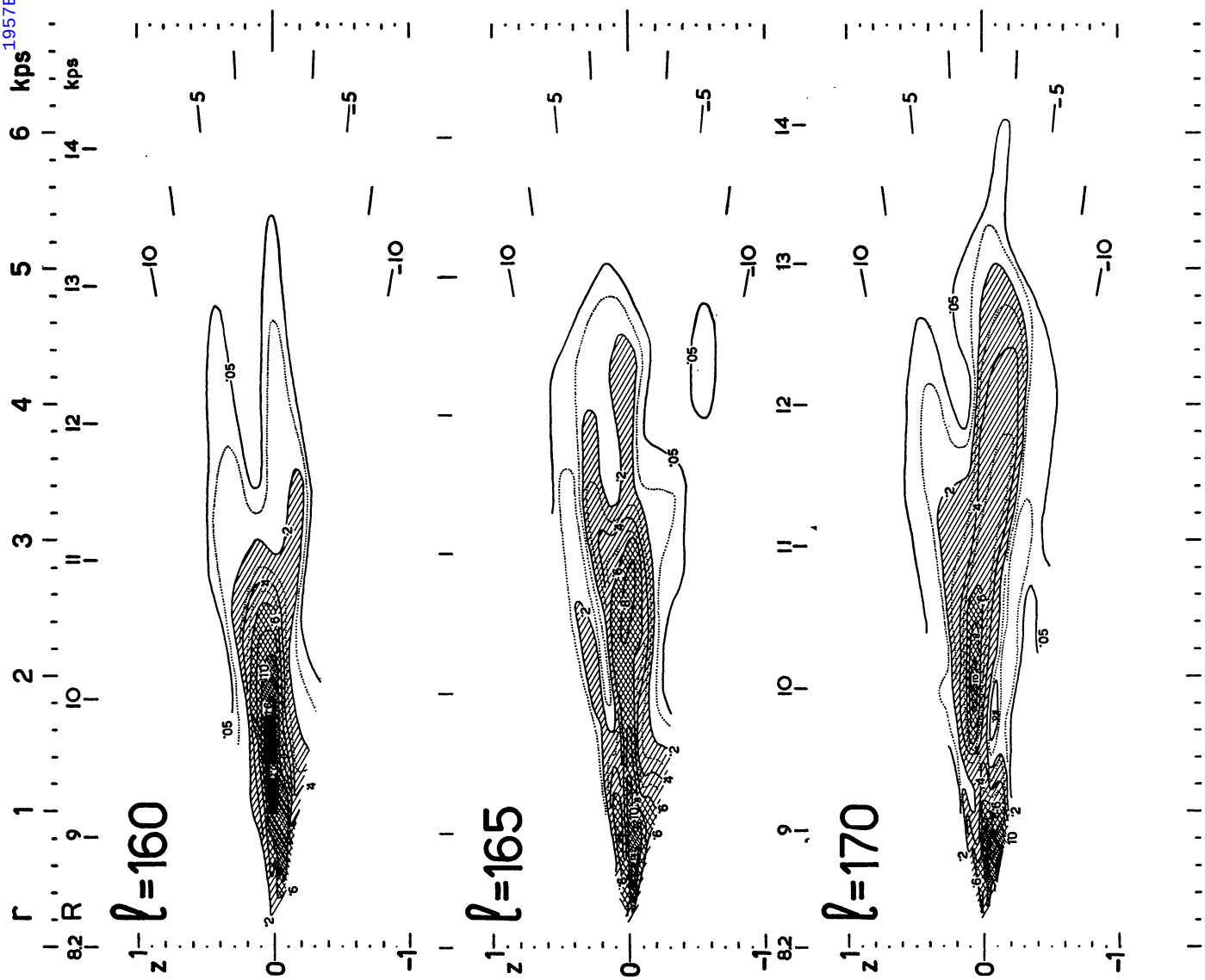

© Astronomical Institutes of The Netherlands • Provided by the NASA Astrophysics Data System

1957BAN....13..201W

FIGURE 9 (*continued*)

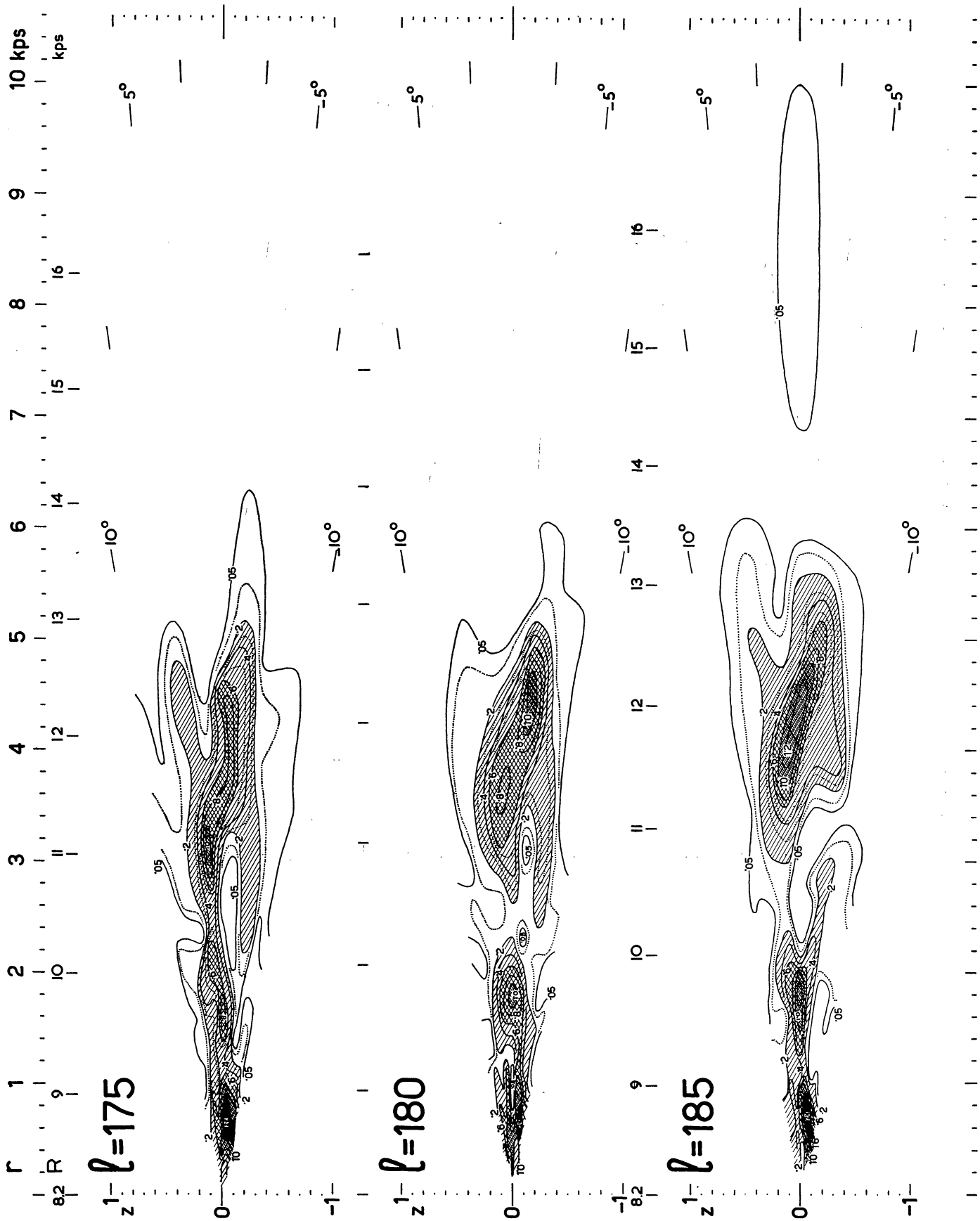

© Astronomical Institutes of The Netherlands • Provided by the NASA Astrophysics Data System

1957BAN....13..201W

FIGURE 9 (*continued*)

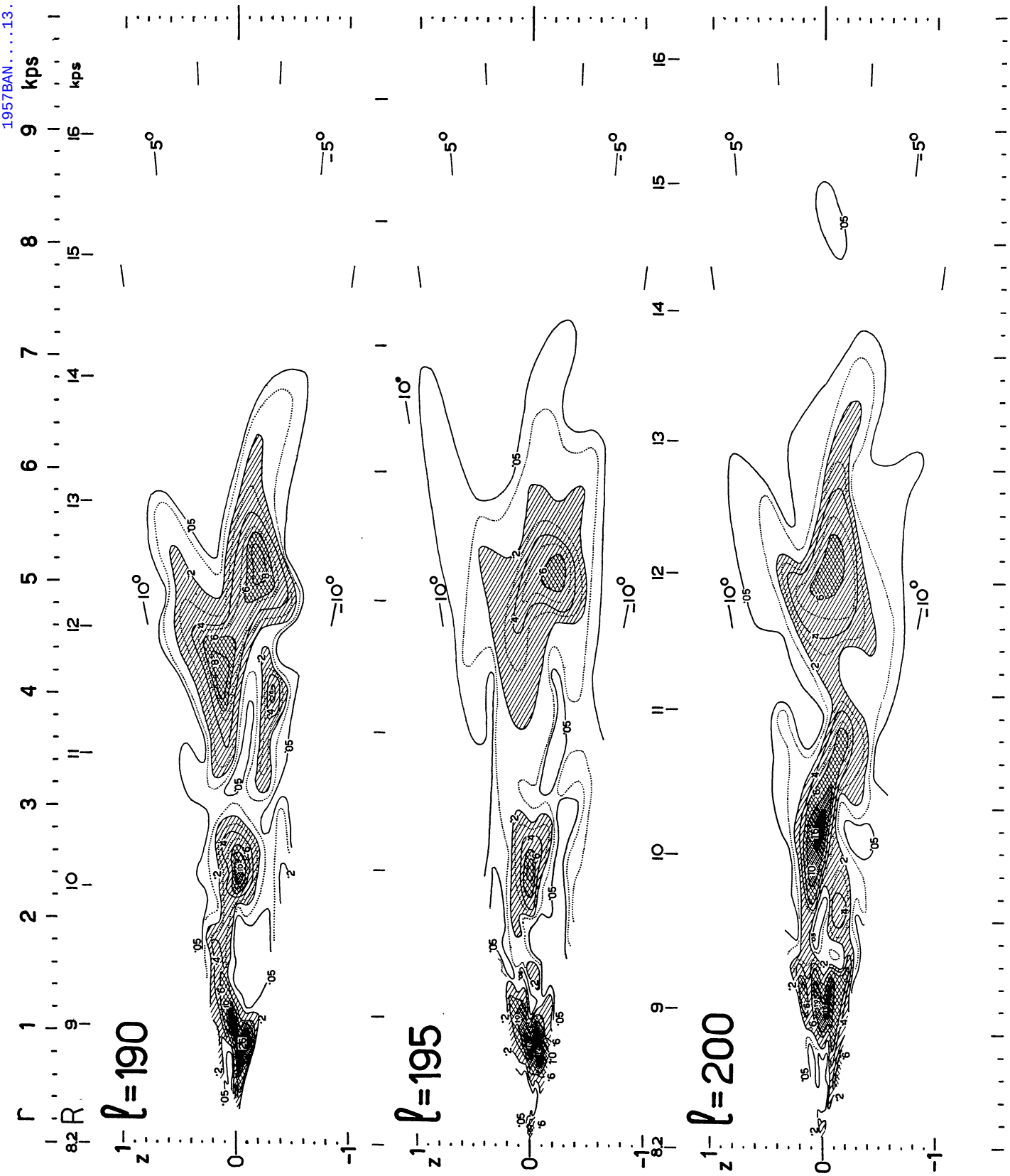

© Astronomical Institutes of The Netherlands • Provided by the NASA Astrophysics Data System

1957BAN...13..201W

FIGURE 9 (*continued*)

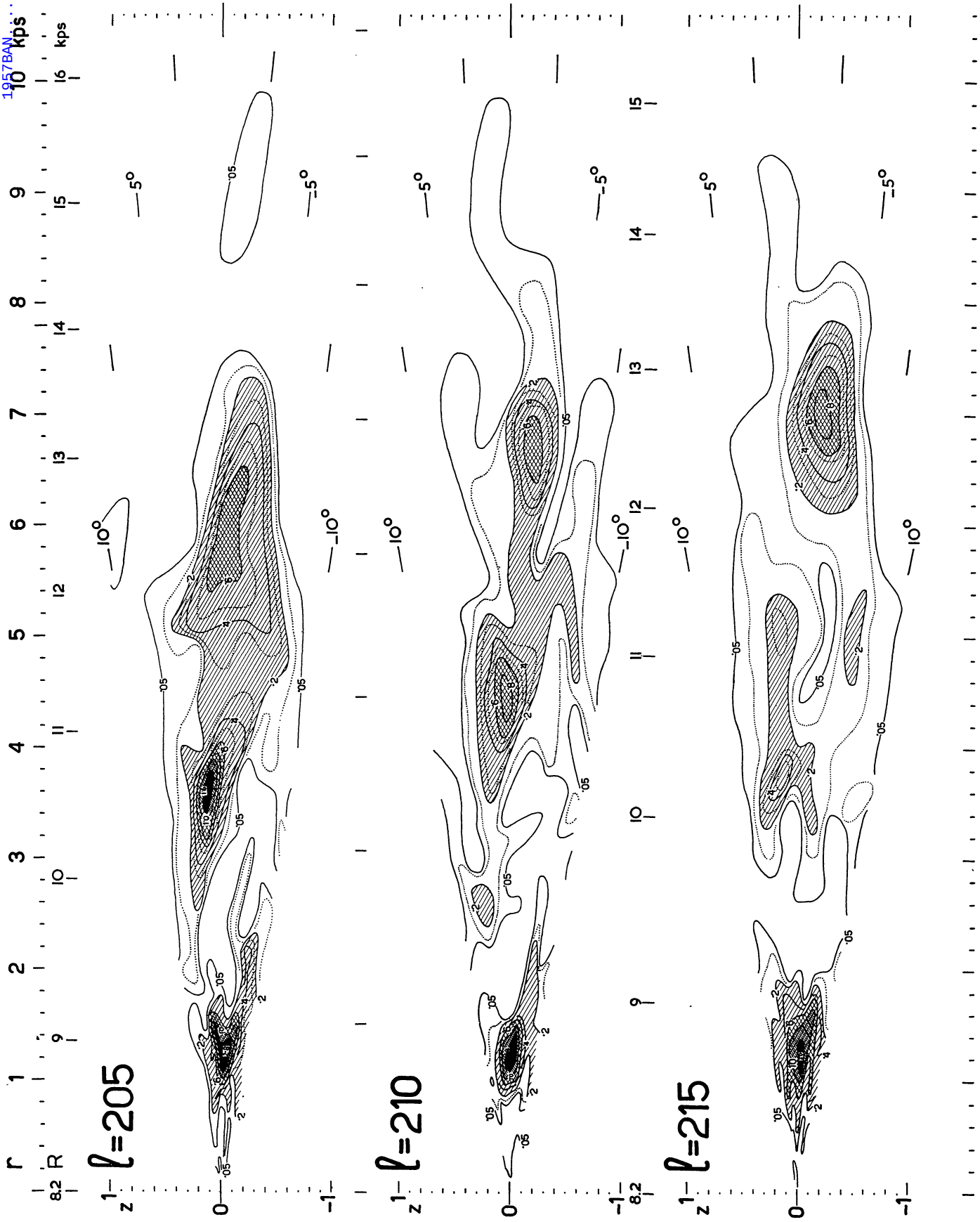

© Astronomical Institutes of The Netherlands • Provided by the NASA Astrophysics Data System